viruses

Article

The Influenza B Virus Victoria and Yamagata Lineages Display Distinct Cell Tropism and Infection-Induced Host Gene Expression in Human Nasal Epithelial Cell Cultures

Jo L. Wilson [1,2,†], Elgin Akin [1,†], Ruifeng Zhou [1], Anne Jedlicka [1], Amanda Dziedzic [1], Hsuan Liu [1], Katherine Z. J. Fenstermacher [3], Richard E. Rothman [3] and Andrew Pekosz [1,*]

1   W. Harry Feinstone, Department of Molecular Microbiology and Immunology, Johns Hopkins University Bloomberg School of Public Health, Baltimore, MD 21205, USA; jo.wilson@pediatrics.wisc.edu (J.L.W.); eakin1@jhu.edu (E.A.); ruifengpotato@gmail.com (R.Z.); ajedlic1@jhu.edu (A.J.); adziedz1@jhu.edu (A.D.); hsuanliu66@gmail.com (H.L.)
2   Division of Allergy, Immunology, and Rheumatology, Department of Pediatrics, Johns Hopkins University School of Medicine, Baltimore, MD 21287, USA
3   Department of Emergency Medicine, Johns Hopkins University School of Medicine, Baltimore, MD 21287, USA; kfenste1@jhu.edu (K.Z.J.F.); rrothma1@jhmi.edu (R.E.R.)
*   Correspondence: apekosz1@jhu.edu; Tel.: +1-410-502-9306
†   These authors contributed equally to this work.

Abstract: Understanding Influenza B virus infections is of critical importance in our efforts to control severe influenza and influenza-related diseases. Until 2020, two genetic lineages of influenza B virus—Yamagata and Victoria—circulated in the population. These lineages are antigenically distinct, but the differences in virus replication or the induction of host cell responses after infection have not been carefully studied. Recent IBV clinical isolates of both lineages were obtained from influenza surveillance efforts of the Johns Hopkins Center of Excellence in Influenza Research and Response and characterized in vitro. B/Victoria and B/Yamagata clinical isolates were recognized less efficiently by serum from influenza-vaccinated individuals in comparison to the vaccine strains. B/Victoria lineages formed smaller plaques on MDCK cells compared to B/Yamagata, but infectious virus production in primary human nasal epithelial cell (hNEC) cultures showed no differences. While ciliated epithelial cells were the dominant cell type infected by both lineages, B/Victoria lineages had a slight preference for MUC5AC-positive cells, and B/Yamagata lineages infected more basal cells. Finally, while both lineages induced a strong interferon response 48 h after infection of hNEC cultures, the B/Victoria lineages showed a much stronger induction of interferon-related signaling pathways compared to B/Yamagata. This demonstrates that the two influenza B virus lineages differ not only in their antigenic structure but also in their ability to induce host innate immune responses.

Keywords: influenza B virus; human nasal epithelial cells; cell tropism; viral transcriptomics; protein immunoassay

1. Introduction

Circulating influenza viruses are members of the family Orthomyxoviridae, with influenza A virus (IAV) subtypes H3N2 and H1N1, and influenza B virus (IBV) Yamagata and Victoria lineages, resulting in the majority of clinically important human infections [1]. The CDC estimates that between 2010 and 2020, seasonal influenza viruses resulted in 9–41 million illnesses, 140,000–710,000 hospitalizations and 12,000–52,000 deaths as of 3 February 2023 [2]. Research on seasonal influenza is biased towards IAV due to IAV accounting for the majority of annual infections. IAV, but not IBV, also poses a pandemic threat due to its ability to infect a wide variety of animal species. IBV is not known to have an animal reservoir, and circulates exclusively in humans [3]. Prior to the SARS-CoV-2 pandemic, IBV represented 20% of confirmed influenza cases and is consistently

underestimated regarding its impact on healthcare burden [4,5]. IAV and IBV infection leads to similar acute clinical syndromes with a wide range of severity [6,7]. Although clinical severity in the general population appears similar across studies, there have been reports of higher IBV-attributable mortality in children and individuals infected with HIV [5,8].

Circulating IBV is divided into two antigenically distinct lineages defined by the Hemagglutinin (HA) genomic segment—B/Victoria/2/1987-like (B/Victoria) and B/Yamagata/16/1988-like (B/Yamagata). In 2012, it was first recommended by the FDA to include both lineages of IBV in a quadrivalent vaccine to replace the trivalent vaccines containing only one IBV lineage [9]. The recommendation was made due to shifting patterns of dominance between IBV lineages resulting in frequent lineage level mismatch as well as limited cross-protection [5,10–13].

Numerous reports in the literature show that these two virus lineages behave differently in the population, suggesting unique features of each that deserve further research. The primary differences noted are patterns of evolutionary escape, variation in predominance based on temperate or tropical climate and age predilection. After 2010, B/Yamagata viruses diversified into multiple, coexisting clades followed by the dominance of a single clade, clade 3, in 2016. B/Yamagata drift has been defined not only by single nucleotide changes in HA but also as driven by single nucleotide changes in neuraminidase (NA). B/Victoria viruses have had high antigenic diversity since 2010 with frequent insertion and deletion events in the HA receptor binding site leading to immune evasion, a strategy observed in B/Victoria evolution since its first isolation [14,15]. There is also a clear difference in age predisposition between these two virus lineages [4,5,16]. B/Yamagata viruses have a higher average age of infection, commonly infecting older adults, whereas B/Victoria viruses show high pediatric rates of infections. One of the highest rates of pediatric mortality attributable to influenza occurred during the 2019–2020 Northern Hemisphere influenza season, where 61% of pediatric deaths were attributable to the B/Victoria lineage despite making up only 41% of total infections (accessed 3 February 2023) [17]. These patterns are well described for IBV; however, the mechanisms that drive these differences remain unknown, highlighting the importance of research to define differences in these virus lineages.

The literature detailing the respiratory epithelium response to IBV infection is limited. Bui et al. published a detailed study of cell tropism and replication kinetics of B/Yamagata and B/Victoria lineage viruses. They showed IBV replication in all human airway organoid cell types (ciliated, mucus-containing, secretory, and basal cells) using immunohistochemistry at 24 and 48 h post-infection (hpi). Using real-time PCR, they evaluate CCXL10, IFN-β, and CCL5 between isolates of B/Yamagata and B/Victoria showing minor strain level differences with no significant lineage level variation. Additionally, clinical evaluations of serum cytokines have shown that IL-17A, IFN-g, and IP-10 are dominant responses after IBV clinical infections [18]. We sought to compare recent clinical isolates from both IBV lineages to define IBV–epithelial cell interactions, including virus replication kinetics, and quantitative cell tropism over the full course of infection using flow cytometry, as well as protein immunoassays and transcriptomics using human primary differentiated nasal epithelial cell cultures with the goal of determining lineage-related differences that might provide insights into IBV circulation.

2. Materials and Methods

2.1. IBV Clinical Isolate Collection from Johns Hopkins Hospital, Baltimore, MD, USA

The human subjects' protocol was approved by the Johns Hopkins School of Medicine Institutional Review Board (IRB90001667) and the National Institutes of Health Division of Microbiology and Infectious Diseases (protocol 15-0103). Patients were enrolled at the Johns Hopkins Medical Institute (JHMI) Department of Emergency Medicine or on inpatient floors. Symptomatic patients in the emergency department were screened and tested for influenza from triage by clinical providers using a validated clinical decision guideline tool.

After written consent was obtained, a nasopharyngeal swab was obtained and stored at $-80\,°C$. A total of 52 IBV samples were collected between 2016 and 2020.

2.2. Cell Lines and Cell Culture Maintenance

Madin-Darby Canine Kidney Cells (MDCK) and MDCK cells overexpressing 2,6 sialyltransferase (MDCK-SIAT-1) were maintained in complete medium (CM) consisting of Dulbecco's Modified Eagle Medium (DMEM) supplemented with 10% fetal bovine serum, 100 U/mL of penicillin and 100 µg/mL of streptomycin mixture (Life Technologies, Carlsbad, CA, USA) and 2 mM Glutamax (Gibco, Billings, MT, USA). Primary Human Nasal Epithelial Cells (Promocell, Heidelberg, Germany) were plated and cultured in Ex-Plus Medium (StemCell Technologies, Pneumacult Ex-Plus Media Kit) without antibiotics. The apical surface of the wells was coated with 0.03 mg/mL Collagen I, Rat Tail (Gibco). One tube of cryopreserved cells (~500,000) was then directly plated on a 24-well transwell plate, with cells divided equally between 24 and 6.5 mm 0.4 µM wells with Ex-Plus media on the apical and basolateral surface. This media promotes proliferation and inhibits terminal differentiation. The media were changed 24 h after cell plating and every 48 h following to maintain cell viability. After 7–10 days, confluence is assessed using visual monitoring by microscopy and objectively measured by Transepithelial Electrical Resistance (TEER). When cell monolayers reached a TEER greater or equal to $400\ \Omega\text{-cm}^2$, both apical and basolateral media were removed and ALI Differentiation media (StemCell Technologies), Pneumacult ALI Basal Medium supplemented with 1X ALI Maintenance Supplement (StemCell Technologies, Cambridge, MA, USA), 0.48 µg/mL Hydrocortisone solution (StemCell Technologies), and 4 µg/mL Heparin sodium salt in PBS (StemCell Technologies) were replaced on the basolateral side only. This change allows full differentiation of human nasal cultures. Media were changed every 48 h to maintain cell viability. The apical surface of cells was intermittently washed with PBS to remove excess mucus. Full differentiation took approximately 4 weeks and cells were considered fully differentiated when there was presence of mobile cilia on the cell surface visible with light microscopy. Cells were used for experiments once considered fully differentiated and remain viable for 4–6 weeks following differentiation. All cells were maintained at $37\,°C$ in a humidified incubator supplemented with 5% CO_2. Influenza B virus infections of hNEC cultures were carried out at $33\,°C$ to model nasopharynx temperature. Plates were placed at $33\,°C$ 24 h prior to infection to acclimate cells to infection temperature.

2.3. IBV Lineage Determination-RT PCR

Nasal swabs from the 2016–2017, 2017–2018, and 2019–2020 seasons that tested positive for IBV rapid PCR in the JH CEIRS database were used. We chose a two-step lineage determination process for IBV-positive PCR nasopharyngeal swabs (Table 1). Lineage was also then confirmed with HA gene segment sequencing. We used WHO-recommended lineage-specific primers and, using RT-PCR, generated oligonucleotides of specific sizes based on lineage [19]. For viruses collected post-2017, we used updated primers to account for observed hemagglutinin deletions at positions 162–164 [20]. Viral RNA was isolated using Qiagen QIAamp Viral RNA Mini Kit per the manufacturer's protocol. In total, 140 µL of nasopharyngeal swab sample was used for each extraction. The concentration of extracted vRNA was measured by NanoDrop and 2 µL of vRNA was input into RT-PCR reactions. One-step RT-PCR master mix was prepared with SuperScript™ III One-Step RT-PCR System with Platinum™ Taq DNA Polymerase per the manufacturer's instruction. All 4 primers were added to the mix at a final concentration of 10 µM.

2.4. Virus Isolation

Nasopharyngeal swabs or nasal wash originating from B/Victoria or B/Yamagata-positive individuals were used for virus isolation on primary cells. The hNEC cultures were washed three times with 150 µL of phosphate-buffered saline (PBS, Gibco) containing 0.9 mM Ca^{2+} and 0.5 mM^{2+} (PBS+), with incubations of 10 min at $37\,°C$ for each wash. In

total, 50 μL of the nasal swab sample was then placed on the apical side of the hNEC cultures and samples incubated at 37 °C for 2 h. Following incubation, the sample was aspirated, and the cells were washed twice with PBS+. Cultures were then incubated at 37 °C. On days 3, 5, and 7 days post-infection, 150 μL of infectious media (IM) consisting of Dulbecco modified Eagle medium (DMEM, Sigma, Tokyo, Japan), 100 U/mL penicillin/streptomycin (Gibco), 2 mM L-glutamine (Gibco), and 0.5% BSA (Sigma) was placed on the apical surface of the cells and incubated for 10 min at 37 °C. The apical wash was harvested and stored at −65 °C, followed by assessment of infectious virus by TCID50 assay.

Table 1. Primers for lineage determination.

Virus Lineage	Primer Name	Sequence
B/Victoria	Bvf224	ACATACCCTCGGCAAGAGTTTC
	Bvr507	TGCTGTTTTGTTGTTGTCGTTTT
B/Yamagata	BYf226	ACACCTTCTGCGAAAGCTTCA
	BYr613	CATAGAGGTTCTTCATTTGGGTTT
Post-2017 B/Victoria	Vic-HA-668R	GAGTCCCCATAGAGCTTTGC
	Vic-HA-472F	TGCCCTAACATTACCAATGG

2.5. TCID50

MDCK-SIAT-1 cells were seeded in a 96-well plate 2 days before assay and grown to 100% confluence. Cells were washed twice with PBS+ then 180 μL of IM was added to each well. Ten-fold serial dilutions of virus from 10^{-1} to 10^{-7} were created and then 20 μL of the virus dilution was added to the MDCK-SIAT-1 cells. Cells were incubated for 6 days at 33 °C then fixed with 2% formaldehyde. After fixing, cells were stained with Naphthol Blue Black, washed and virus titer was calculated using the Reed and Muench method [21].

2.6. Virus Seed and Working Stocks

The earliest clinical isolate sample that showed presence of infectious virus was selected. A T75 flask of confluent MDCK-SIAT-1 cells was infected at an MOI of 0.01. Working stocks for each clinical isolate were generated by infecting a T75 flask of MDCK-SIAT-1 cells at an MOI of 0.001 for one hour at room temperature while rocking. The inoculum was removed, and cells were placed in a 33 °C incubator and monitored daily for CPE. Working stock was harvested between 3 and 5 days later, when CPE was seen in 75–80% of the cells. Harvested media were centrifuged at $400 \times g$ for 10 min at 8 °C to remove cell debris, and the resulting supernatant was aliquoted into 500 μL and stored at −80 °C infectious virus quantity of working stocks was determined using TCID-50 assay. Seed and working stocks of the egg-adapted vaccine strains of IBV (see Table 2) were grown directly in MDCK-SIAT-1 cells as described above. IBV vaccine strains were kindly provided by Johns Steel, Centers for Disease Control (CDC).

Table 2. Viruses used in comparison studies.

Virus Lineage/Clade	Source	Virus Name	GISAID Accession
Victoria/V1A	Clinical isolate	B/Baltimore/R0122/2016	EPI_ISL_17412143
Victoria/V1A	Clinical isolate	B/Baltimore/R0001/2016	EPI_ISL_17412142
Yamagata/Clade 3	Clinical isolate	B/Baltimore/R0250/2018	EPI_ISL_17412144
Yamagata/Clade 3	Clinical isolate	B/Baltimore/R0337/2018	EPI_ISL_17412145
Yamagata/Clade 3	Clinical isolate	B/Baltimore/R0300/2018	EPI_ISL_17742639
Victoria/V1A.1	Vaccine (CDC)	B/Colorado/06/2017	EPI_ISL_257735
Victoria/V1A.3	Clinical isolate	B/Baltimore/R0696/2019	EPI_ISL_17353886
Yamagata/Clade 3	Vaccine (CDC)	B/Phuket/3073/2013	EPI_ISL_161843

2.7. HA Sequencing and Lineage Assignment

Vaccine virus HA segments were sequenced to confirm that no sequence alteration occurred with the creation of working stocks. A 100% sequence identity was maintained

using the GISIAD sequence database for sequence comparison. Viral RNA from each sample was isolated using Qiagen vRNA isolation Kit. Superscript III RT-PCR system (ThermoFisher, Waltham, MA, USA) was used to isolate cDNA for sequence analysis. Primers were designed at the 5′ and 3′ noncoding regions HA segment with the goal of sequencing the entire segment (Table 3).

Table 3. Primer design.

Primer Lineage	Primer Name	Primer Sequence
B/Yamagata RT-PCR primer	IBV_Yam_5UTR_1F	AGCAGAAGCAGAGCATTTTCT
	IBV_Yam_3UTR_1842R	TGATGACAAGCAAACAAGCACT
B/Victoria RT-PCR primer	IBV HA 5′ UTR	TATTCGTCTCAGGGAGCAGAAGCA GAGCATTTTCT
	IBV HA 3′ UTR R	GTAATGATGACAAGCAAACAAGCA

Additional sequencing primers were designed within the reading frame to ensure full coverage of the entire segment. The cDNA was sent to the Synthesis and Sequencing Facility of the Johns Hopkins University for Sanger sequencing.

2.8. Influenza B Genome Sequencing

Viral RNA was extracted using the QIAamp viral RNA mini extraction kit. For library preparation, the Illumina RNA Prep with Enrichment (L) Tagmentation kit with Respiratory Virus Oligo Panel v2 (20044311) was used following the single-plex enrichment protocol, and samples were sequenced using a MiSeq Illumina sequencer (v3, 2 × 300 bp or 2 × 75 bp). Consensus sequences were generated using the DRAGEN RNA Pathogen Detection pipeline using custom .bed files and FASTA files for IBV.

2.9. HA and NS Phylogenetics Analysis

Representative IBV HA and NS sequences between 2009 and 2022 were accessed from GISAID filtered to include only complete sequences [22]. Associated GISAD metadata for HA and NS sequences analyzed in this study are compiled in Supplemental Table S4. Sequences were aligned using MAFFT v7.520. For the HA tree, amino acid changes were standardized using HA numbering using the FluDB conversion tool. Alignments were used to construct a maximum likelihood time-resolved tree in treetime using a relaxed molecular clock model. Clade assignments for B/Victoria and B/Yamagata were assigned using NextClade v2.11.0 with the influenza B lineage workflows. Constructed trees were annotated by lineage and clade in R v4.1.1 using ggtree v3.16 [23,24].

2.10. Neutralizing Antibody Assays

Serum samples used for this analysis originated from Johns Hopkins Medical Institute healthcare workers recruited from the Johns Hopkins Centers for Influenza Research and Surveillance (JHCEIRS). Recruitment occurred during the annual employee influenza vaccination campaign in the Fall of 2019. Participants were vaccinated with split inactivated quadrivalent vaccine formulations. Influenza vaccination is required of all HCWs at Johns Hopkins University and, therefore, most of the study participants have had an influenza vaccine over the past three years. Pre-vaccine and approximately 28-day post-vaccination samples were used for analysis. Subjects provided written informed consent prior to participation. The JHU School of Medicine Institutional Review Board approved this study, IRB00288258. Serum samples were first treated (1:3 ratio serum to enzyme) with Receptor Destroying Enzyme (Denka-Seiken, Tokyo, Japan) and incubated overnight at 37 °C followed by inactivation at 57 °C for 35 min. Serum was diluted 2-fold in IM (Dulbecco modified Eagle medium (Sigma), with 10% penicillin/streptomycin (Gibco), 10% L-glutamine (Gibco), 0.5% BSA (Sigma), and 5 μg/mL of N-acetyl trypsin (Sigma) at 37 °C and 5% CO_2) and 100 TCID50 was added for a one-hour incubation at room temperature. Serum Sample/Virus was used to infect a confluent layer of MDCK-SIAT-1

cells. The inoculums were removed after 24 h, IM was replaced, and cells were incubated for 96 h at 37 °C. Plates were fixed and stained as described previously. The Neutralizing Antibody titer was calculated using the highest serum dilution that led to greater than 50% CPE. Statistical analysis was completed comparing means of pre and post-neutralzing responses as well as between lineages. Mean differences were calculated and Sidak's multiple comparisons test was used to assess significant differences. Statistical differences were set at $p \leq 0.05$.

2.11. Plaque Assays

MDCK cells were grown in complete medium to 100% confluency in 6-well plates. Complete medium was removed, cells were washed twice with PBS containing 100 µg/mL calcium and 100 µg/mL magnesium (PBS+) and 250 µL of inoculum was added. Virus dilution was conducted by serially diluting the virus stock 10-fold each time until 10^{-6}. Cells were incubated at 33 °C for 1 h with rocking every 10 min. After 1 h, the virus inoculum was removed and phenol-red free MEM supplemented with 3% BSA (Sigma), 100 U/mL of penicillin and 100 µg/mL of streptomycin mixture (Life Technologies), 2 mM Glutamax (Gibco), and 5 µg/mL N-acetyl trypsin (Sigma), 5 mM HEPES buffer and 1% agarose was added. Cells were incubated at 33 °C for 3–5 days and then fixed with 4% formaldehyde. After removing the agarose, cells were stained with Naphthol Blue Black. Plaque size was analyzed in Image J.

2.12. Low-MOI Infections

Low-MOI growth curves were performed at an MOI of 0.01 in hNEC cultures. The hNECs were acclimated to 33 °C for 48 h before infection. The apical surface was washed three times with PBS and the basolateral media were changed at time of infection. hNEC cultures were inoculated at an MOI of 0.01. hNEC cultures were then placed in a 33 °C incubator for 2 h. After incubation, the apical surface of the hNEC culture was washed three times with PBS+. At the indicated times, 100 µL of IM without N-acetyl trypsin was added to the apical surface of the hNECs for 10 min at 33 °C, the IM was harvested and stored at −80 °C. Basolateral media were changed every 48 h post-infection for the duration of the experiment. Infectious virus titers in the apical supernatants were measured with TCID50 assay.

2.13. Flow Cytometry

For the 72 h time point experiments, hNEC cultures were infected with IBV clinical isolates at an MOI of 0.01 for 72 h (Tables 4 and 5). At this time point, cells from both infected samples and uninfected controls were harvested, creating a single-cell suspension after a 30 min incubation in 1X TrypLE. The cells were then resuspended in trypsin stop solution, washed, and resuspended in 1X PBS. All washes were carried out between blocking, primary, secondary or conjugated antibody staining using either 1X PBS or BD Perm/Wash Buffer (after Fixation/Permeabilization) at a centrifuge speed of $400 \times g$ at 4 °C. Samples and controls were stained with AQUA viability dye (1 µL/1 $\times$ 10^6 cells) for 30 min at room temperature (RT). Following staining, cells were washed and resuspended in BD Fixation/Permeabilization solution, and they were incubated for a minimum of 30 min at 4 °C. Cells were blocked with 7% normal goat serum in BD Perm/Wash Buffer for 1 h at 4 °C. Next, cells were incubated with primary antibodies and diluted in BD Perm/Wash buffer at appropriate concentrations for one hour at RT. Subsequently, cells were incubated with secondary antibodies, as described for the primary antibodies, for 30 min at RT. After secondary antibody staining, the same procedure was repeated for incubation with conjugated antibodies for 30 min at RT. Cells were finally resuspended in FACS Buffer and filtered through a 35 µM strainer cap into FACS tubes.

Stained suspensions were analyzed using a BD LSRII Flow Cytometer with DIVA software v7.0. The following laser-emission filter-(fluorochrome groupings) were used: 488 nm-530/30-(AF488,PE), 633 nm-660/20-(AF647), 405 nm-525/50-(AQUA/BV605). Con-

trols included single stained cells, fluorescence minus one controls for gating assistance, secondary antibody alone controls, and uninfected IBV HA stained controls to ensure absence of non-specific staining. Data analysis was conducted using FlowJo v10. The gating strategy consisted of excluding debris, selecting single cells, and identifying aqua-negative cells (LIVE).

Table 4. Antibody list.

Antibody/Probe/Clone	Fluorophore	Catalog Number	Staining Concentration
Flow cytometry [1]			
Recombinant Rabbit HA Monoclonal	Primary	Invitrogen MA5-29901	1 μg/mL
MUC5AC Monoclonal Antibody Clone: 45M1	Primary	Invitrogen MA5-12178	2 μg/mL
CD271 (NGF Receptor) Monoclonal Antibody (ME20.4), PE, eBioscience	Conjugated-PE	Invitrogen 12-9400-42	0.5 μg/mL
Goat Anti-Rabbit (Secondary for HA probe)	AF647	Invitrogen A21244	2 μg/mL
Goat Anti-Mouse (Secondary Ab for MUC5AC probe) Clone: Poly4503	BV605	Biolegend 405327	0.2 μg/mL
Mouse Anti-Beta Tubulin-IV	AF488	Novus Bio NBP2-74713AF488	0.78 μg/mL
Live/Dead Discriminator	AQUA	Invitrogen L34965	1 mL/10^6 cells
Western blots			
Rabbit IFIT2	Primary	Protein Tech 12604-1-AP	2 μg/mL
Rabbit IFIT3	Primary	Protein Tech 5201-1-AP	1 μg/mL

[1] Instrument: BD LSRII, software: DIVA v7.0.

Table 5. Flow cytometry reagent list.

Reagent	Catalog Number
TrypLE 1X	Gibco 12563011
BD Fixation/Permeabilization Kit (Cytofix/Cytoperm and Perm/Wash Buffer)	BD Biosciences 554714
Normal Goat Serum (NGS)	Sigma Aldrich G9023
FACS Buffer: 0.3% BSA in 1X PBS	BSA: Sigma Aldrich A9418, PBS PH 7.4: Gibco 10010072
Trypsin Stop Solution (10% FBS in PBS)	FBS: Thermofisher, Gibco, Lot:2193952RP

For the time-course experiment, a low MOI infection was carried out at an MOI of 0.01. At each designated time point (72 h post-infection, 96 h post-infection, and 120 h post-infection), cells were trypsinized, stained to discriminate live/dead cells, and then fixed in 4% formaldehyde according to the aforementioned protocol. After fixation, the samples were stored at 4 °C until all samples were collected. Following this, the samples were collectively blocked and stained as previously described, and the LSRII was used for analysis.

2.14. Luminex Assays

To evaluate cytokine and chemokine responses to infection, a custom 22-plex Luminex panel for the MagPix instrument was designed for pre-validated cytokine and chemokine targets using the Thermofisher ProcartaPlex Panel Configurator (Catalog Number: PPX-22-MXAACRC, Bead/Plate Lot #: 307393-000/305694-000). The following analytes were selected: BAFF, E-Cadherin, Eotaxin-3, Eotaxin, G-CSF, IFN-a, IL-6, IL-18, MCP-1, MCP-4, MDC, MIP-1-a, MIP-1-b, MIP-2-a, TARC, TGF-a, TNF-a, TRAIL-R1, TSLP, VEGF-A, IP-10 and IL-8. Infections were completed with IBV working stocks at a low MOI (0.01) on hNECs. The basolateral media were changed at time zero of the infection. Basolateral samples were collected from the infection at 48 hpi and 96 hpi. Uninfected mock basolateral media were collected at identical time points. Samples were run on the custom Procartaplex assay plates with appropriate standards and controls according to manufacturer instruc-

tions on a Luminex MagPix System. Raw data were exported and analyzed using ThermoFisher Procartaplex Software and visualized by log fold change to mock in R v4.1.1 using custom scripts.

2.15. RNAseq and Analysis

Total RNA at 48 hpi was extracted and purified from hNECs using Trizol reagent (Invitrogen Catalog # 15596018) and the PureLink RNA Mini kit, including on-column DNAse treatment (Invitrogen/ThermoFisher, Waltham, MA, USA). Quantitation of total RNA was performed with the Qubit BR RNA Assay kit and Qubit Flex Fluorometer (Invitrogen/ThermoFisher), and quality assessment was performed by RNA ScreenTape analysis on an Agilent TapeStation 2200. Unique Dual-index Barcoded libraries for RNA-Seq were prepared from 100 ng total RNA using the Universal Plus Total RNA-Seq with NuQuant Library kit (Tecan Genomics), according to manufacturer's recommended protocol. Library amplification was performed for 16 cycles, as optimized by qPCR. Quality of libraries was assessed by High Sensitivity DNA Lab Chips on an Agilent BioAnalyzer 2100. Quantitation was performed with NuQuant reagent, and confirmed by Qubit High Sensitivity DNA assay, on Qubit 4 and Qubit Flex Fluorometers (Invitrogen/ThermoFisher). Libraries were diluted, and equimolar pools were prepared, according to manufacturer's protocol for the appropriate sequencer. An Illumina iSeq Sequencer with iSeq100 i1 reagent V2 300 cycle kit was used for final quality assessment of the library pool. For deep RNA sequencing, a 200-cycle (2 × 100 bp) Illumina NovaSeq S2 run was performed at Johns Hopkins Genomics, Genetic Resources Core Facility, RRID:SCR_018669. Unaligned FASTQ files and .bam files are available under NCBI BioProject: PRJNA996592.

2.16. Sequencing Analysis

Raw iSeq and NovaSeq FASTQ files were uploaded to the Partek Server and analysis with Partek Flow® (Version 10.0) next-generation sequencing software, with RNA Toolkit, was performed as follows: pre-alignment QA/QC; trimming of reads; alignment to hg38 Reference Index using STAR 2.7.8a; post-alignment QA/QC; quantification of gene counts to annotation model (Partek E/M, Ensembl Transcript Release 103). Gene count matrices were exported from the Partek server and further analysis in R v4.1.1. Gene counts were log-transformed for normalized analysis using base R rlog. Principle component analysis (PCA) of normalized gene counts was performed using the plotPCA function from DESeq2 [25]. Differentially Expressed genes were determined using DESeq2 with alpha set to 0.05 for adjusted *p*-value (padj) thresholding. A gene was differentially expressed at a padj ≤0.05. DEGs were then summarized by a log2fold change of ≥1.5. Gene set enrichment analysis was performed using gprofiler [26].

Interferon-stimulated gene targets identified by RNAseq were performed. Whole RNA was isolated using TRIzol Plus RNA Purification Kit (Cat #: 12183444). Three wells of whole cell lysates of hNECs per virus and mock were used for each extraction. Direct RNA was used to run premixed TaqMan primers and probes for each virus in separate reactions for targets IFITM1, ZPB1, and OASL (Table 6) using TaqPath 1-Step RT-qPCR Master Mix, CG (Thermofisher Cat# A15299). Standard thermal cycling conditions were performed on a QuantStudio 5 Instrument as follows: 1 cycle of Reverse transcription at 50 °C for 15 min, 1 cycle of Polymerase activation at 90 °C for 2 min, and 40 cycles of 95 °C for 3 s to 60 °C for 30 s of amplification. Analysis was performed using QuantStudio design analysis software v1.3 and statistical significance between groups was tested using 2-way ANOVA in Graphpad Prism.

2.17. Western Blots

Low MOI infections (MOI = 0.01) were performed in hNECs. Cells were extracted using TrypLE (Thermofisher Scientific Cat no. 12604013) and lysed using RIPA buffer (Thermofisher Cat no. 89900). Sample lysates were stained with antibodies raised in rabbit against IFIT2 and IFIT3 with Beta Tubulin-IV as a control (Table 4). Fluorescent

Secondary staining was performed using fluorophore-conjugated antibodies AF647 raised in goat and anti-mouse AF488 raised in goat for IFIT2 or 3 and Beta Tubulin-IV primary antibodies, respectively.

Table 6. Interferon gene RT-qPCR—RT qPCR primers.

Target	Assay	Assay ID
IFITM1	Thermofisher TaqMan	Hs00705137_s1
ZPB1	Thermofisher TaqMan	Hs01679797_gH
OASL	Thermofisher TaqMan	Hs00984387_m1

2.18. Data Availability

All RNAseq raw sequence files, .bam files and sample information have been deposited at NCBI Sequence Read Archive, NCBI BioProject: PRJNA996592. All scripts used for RNAseq analysis are available at https://github.com/Pekosz-Lab/IBV_transcriptomics_2023 (accessed on 14 March 2023). Raw data used in this manuscript can be obtained through the Johns Hopkins Data Repository at doi: 10.7281/T1/EQKCFP. All genome sequences and associated metadata in this dataset are in the GISAID EpiFlu database. To view the contributors of each individual sequence with details such as accession number, nirus name, collection date, originating lab, submitting lab and the list of authors, please refer to Supplemental Table S4.

3. Results

*3.1. Maryland Influenza B Clinical Frequency and Hemagglutinin (HA) Phylogenetic Assessment*

Clinical prevalence of IBV in the United States from 2015 to 2020 showed a prevalence of the B/Yamagata lineage until the 2019–2020 season, when the B/Victoria lineage dominated (Figure 1A). Approximately 20 nasal swabs from each lineage were screened during this time and three clinical isolates from each IBV lineage were chosen for further characterization, as labeled in Figure 1B. In order to determine the relative genetic distance of influenza viruses used in this study to historical and circulating viruses, we performed phylogenetic analysis of the hemagglutinin (HA) using genetically representative sequences obtained from GISAID between 2009 and 2023. A total of 285 complete IBV HA sequences were obtained with accession numbers available in Supplemental Table S4. Maximum-likelihood phylogenetic tree construction of GISAID sequences and HA segments of clinical isolates revealed distinct clustering by lineage and clade (Figure 1B). B/Victoria used in this study isolated in 2017, B/Baltimore/R0122/2017 and B/Baltimore/R0001/2017, belong to the V1A clade. B/Baltimore/R0696/2020 isolated in 2020 belongs to V1A.3a. All B/Yamagata isolates, B/Baltimore/0300/2018, B/Baltimore/R0250/2018 and B/Baltimore/R0337/2018, belong to the Y3 clade.

3.2. B/Yamagata Vaccines Induce Higher Mean Post-Vaccination Titers Compared to B/Victoria Vaccines in the 2019/2020 Season

A comparison of post-influenza-vaccination neutralizing antibody titers using serum collected from influenza-immunized healthcare workers at Johns Hopkins University during the 2019–2020 season was performed to assess how vaccine-induced immunity recognized the circulating IBV strains. All participants received quadrivalent inactivated vaccine. Neutralizing antibody titers were compared pre and post-vaccination to the vaccine strains and the IBV clinical isolates representing the dominant circulating strains. For B/Yamagata, that was clade 3 (B/Baltimore/R0250/2018) which is in the same subclade as the vaccine (B/Phuket/3073/2013). For B/Victoria, there was an antigenic drift that season and therefore the dominant circulating strain was clade V1A.3 (B/Baltimore/R0696/2019) compared to the vaccine strain, V1A.1 (B/Colorado/06/2017).

Post-vaccination neutralizing antibody titers were significantly higher against all viruses tested (Figure 2A). The post-vaccination mean neutralizing antibody titers were higher for the B/Yamagata vaccine component compared to the B/Victoria component, and

titers against the circulating IBV strains were lower compared to the vaccine strain from the same lineage (Figure 2A). Post-vaccination titers were higher for the vaccine strains when compared to the circulating viruses in the same lineage. Seroconversion rates, defined as a greater than four-fold increase between pre- and post-vaccination sera, were slightly higher for the vaccine strains compared to the circulating viruses, but these differences did not reach statistical significance (Figure 2B). Together, the data indicate this population had a strong response to influenza vaccination but that the vaccine-induced antibodies recognized the vaccine strains better than the circulating strains.
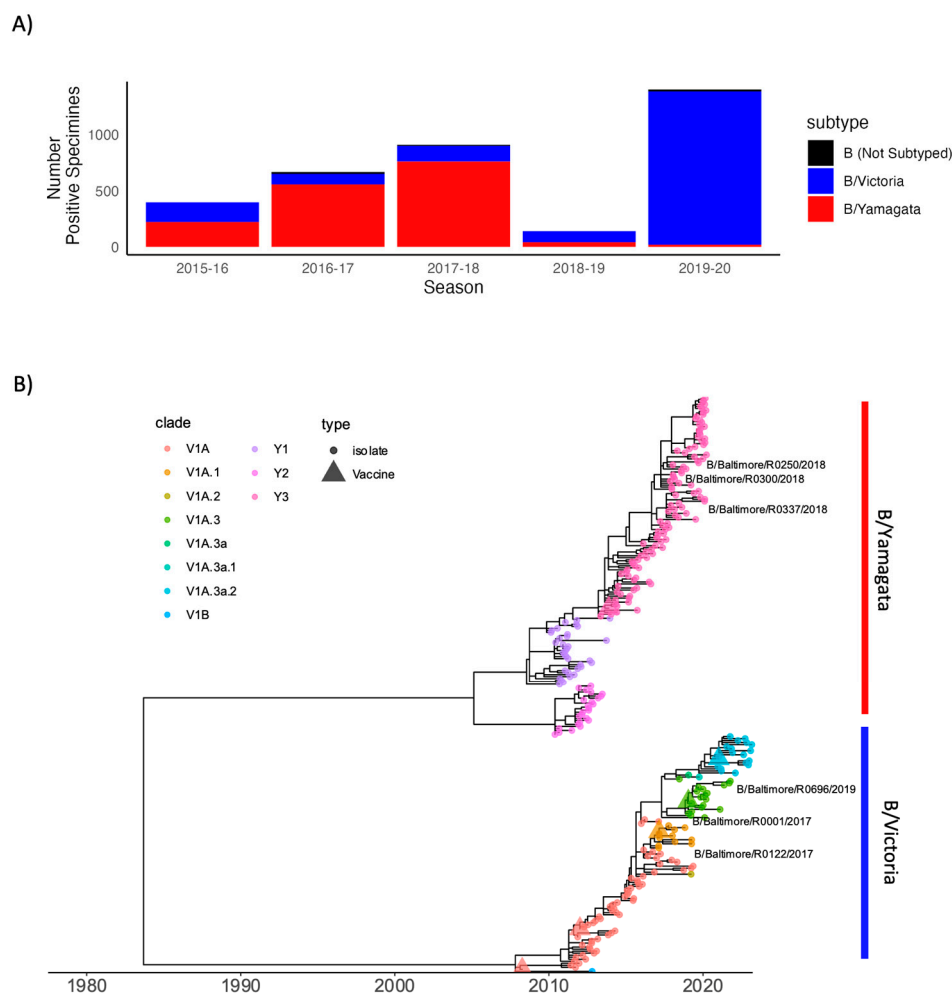
Figure 1. Influenza B clinical incidence and HA phylogenetics. (**A**) Number of influenza B positive clinical specimens as reported by the Centers for Disease Control and Prevention in the State of Maryland from the 'WHO NREVSS Public Health Labs' FluView dataset. Data are summarized by lineage and influenza season. (**B**) Time-scaled phylogenetic tree of influenza tree of representative HA sequences (*n* = 282) isolated between 2009 and 2023. Branch tips are colored by lineage with corresponding vaccine strains defined by tip shape. Isolates collected from the Johns Hopkins Hospital network for subsequent characterization in this study are labeled by isolate ID.

3.3. Viral Production Is Similar between B/Victoria and B/Yamagata Viruses Isolated between 2016 and 2019

The serological data suggested that both IBV lineages could evade pre-existing or vaccine-induced immunity to a similar level, suggesting that lineage-specific differences in virus replication kinetics might help explain the dominance of the B/Yamagata lineage in the 2016–2017 and 2017–2018 influenza seasons (Figure 1A). We chose to use low MOI growth curves to compare infectious virion production over the course of 4 days as a comparison of replication efficiency between lineages. Low MOI infections of the two

lineages of IBV showed similar onset of infection as well as peak infectious virus titer in human nasal epithelial cells (hNECs) (Figure 3A).
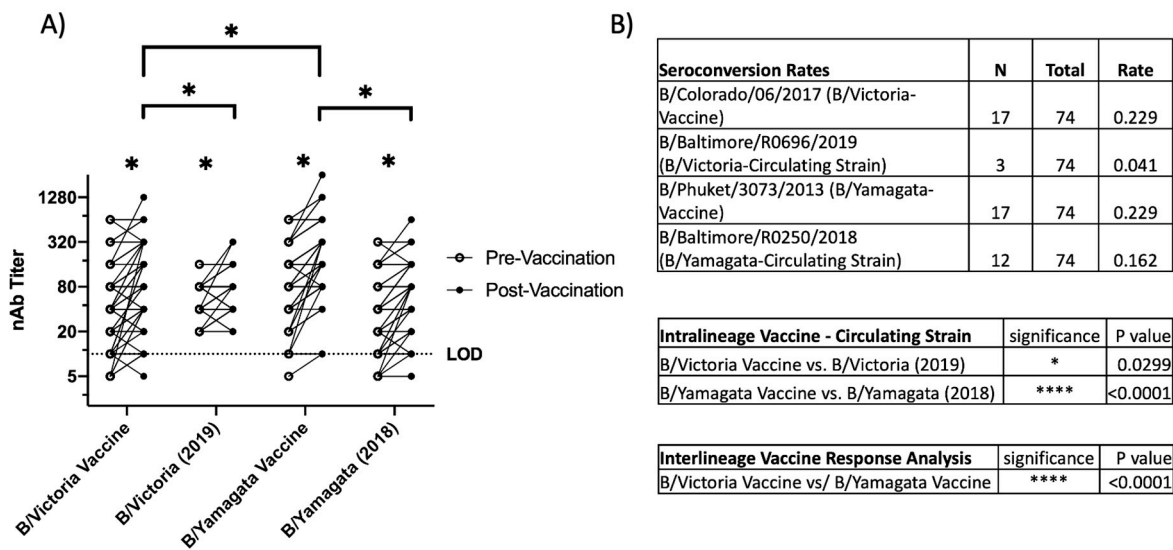
Figure 2. Neutralizing antibody responses to vaccination. (**A**) Neutralizing antibody titers to pre and post-vaccination sera. Pre- and post-vaccination sera were used to compare the neutralization of B/Yamagata and B/Victoria vaccine strains (B/Phuket/3073/2013 and B/Colorado/06/2017) as well as B/Yamagata and B/Victoria circulating strains for the year 2019–2020 (B/Baltimore/R0250/2018 and B/Baltimore/R0696/2019). (**B**) Mean difference was calculated, and Sidak's multiple comparisons test was used to assess significant differences. Statistical differences set at $p \leq 0.05$ and indicated by *. **** $p < 0.0001$.

3.4. B/Yamagata Viruses Show Consistently Larger Plaque Formation on MDCK Cells

Plaque size and morphology is a common technique used to evaluate viral phenotype. Plaque formation allows an assessment of cell-to-cell spread in the MDCK cell model. We directly compared IBV plaque formation between the B/Victoria and B/Yamagata lineage viruses. B/Victoria viruses consistently show smaller plaque size (Figure 3B,C) compared to B/Yamagata viruses ($p < 0.0001$).

3.5. Influenza B Viruses Infect Multiple Types in the Nasal Respiratory Epithelium but Predominate in the Ciliated Cells

Bui et al. used immunohistochemistry (IHC) to show that IBV clinical isolates from both lineages infect multiple cell types in the bronchial respiratory epithelium. We sought to define cell tropism in our hNEC model. Using flow cytometry, we can gain a quantitative view of IBV infection over the initial five days of infection. IBV-infected hNECs were isolated by first gating out debris, multiplets and dead cells followed by gating of IBV HA-positive cells (Figure 4A). We used intracellular markers commonly used to describe various cell types in the respiratory epithelium. Beta-Tubulin-IV (BT-IV) was used to define mature ciliated cells [27,28]. The hNEC cultures showed three populations of BT-IV staining (Supplemental Figure S1A). Total populations include a negative staining population, an intermediate population and a BT-IV positive population. When fluorescence was plotted against the side scatter area (SSC-A), a distinct rise in the population with the highest fluorescence was seen consistent with developing cilia (Supplemental Figure S1A). MUC5AC was used as the intracellular target to identify mucus-producing cells [29]. This would encompass both goblet cells as well as ciliated cells that produce mucus as has been well defined in the literature (Supplemental Figure S1A) [30,31]. NGFR (CD271) was used as a marker for respiratory basal cells [28]. NGFR staining in our hNEC cultures did not show any significant co-staining with the brightest BT-IV population defined as ciliated cells or MUC5AC-containing cells consistent with expected protein production in these

developing cell types (Supplemental Figure S1B,D). Once these cell types were identified, we used this method to identify quantitative IBV cell tropism of our infected hNEC cultures. At peak infectious virus production, 72 hpi, the majority of IBV-infected cells were ciliated cells (B/Victoria 54.77% and B/Yamagata 52.18%, $p = 0.599$) followed by mucus-producing cells (B/Victoria 35.45%, B/Yamagata 39.04, $p = 0.155$) and basal cells (B/Victoria 4.81, B/Yamagata 11.06, $p = 0.0045$) (Figure 4B). There was no significant variation between lineages in the ciliated cell or mucus-producing cell populations. B/Yamagata viruses infected significantly higher NGFR + basal cells compared to B/Victoria (Figure 4B).
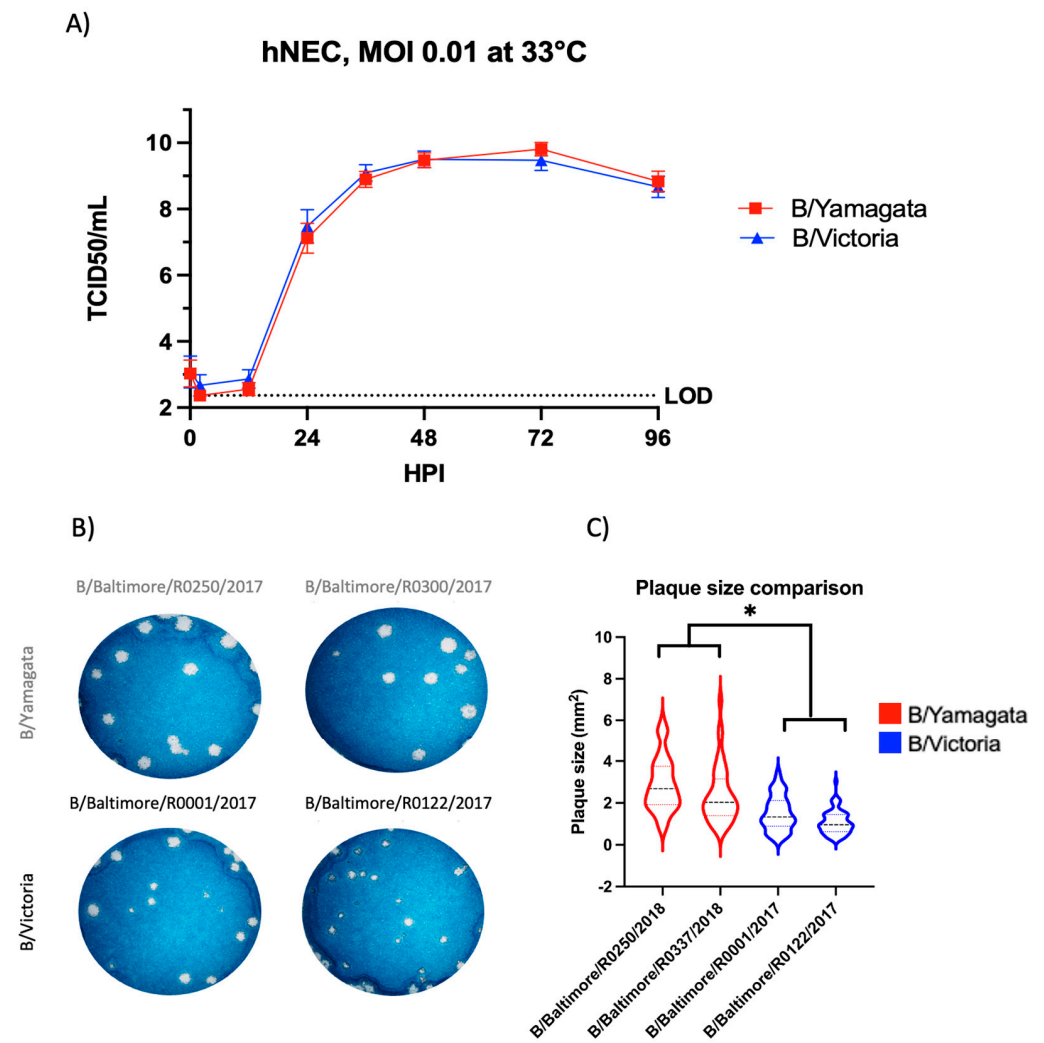
Figure 3. Characterization of viral fitness between B/Yamagata and B/Victoria viruses. (**A**) Viral fitness assessment on hNEC revealed no significant difference in infectious virus production out to 96 h post-infection of Baltimore clinical isolates. B/Yamagata curves consists of data from B/Baltimore/R0250/2018 and B/Baltimore/R0337/2018 clinical isolates. B/Victoria curves consist of data from B/Baltimore/R0001/2017 and B/Baltimore/R0122/2017. Growth curves completed in two independent experiments, each experiment consisted of three replicate wells. Statistical significance of growth curves calculated on GraphPad Prism using a two-way ANOVA and Tukey's multiple comparisons. (**B**) Representative wells shown comparing plaque size from two independent experiments of the two lineages of IBV on MDCK cells. All plaques in experiment wells were counted for analysis. (**C**) Comparison of plaque sizes formed by two clinical isolates from each IBV lineage. Graphed plaque areas are the combination of two independent experiments. Images of plaques were analyzed with ImageJ. Statistical significance of plaque assays calculated on GraphPad Prism using a two-way ANOVA and Tukey's multiple comparisons. * denotes statistical significance of $p < 0.05$.
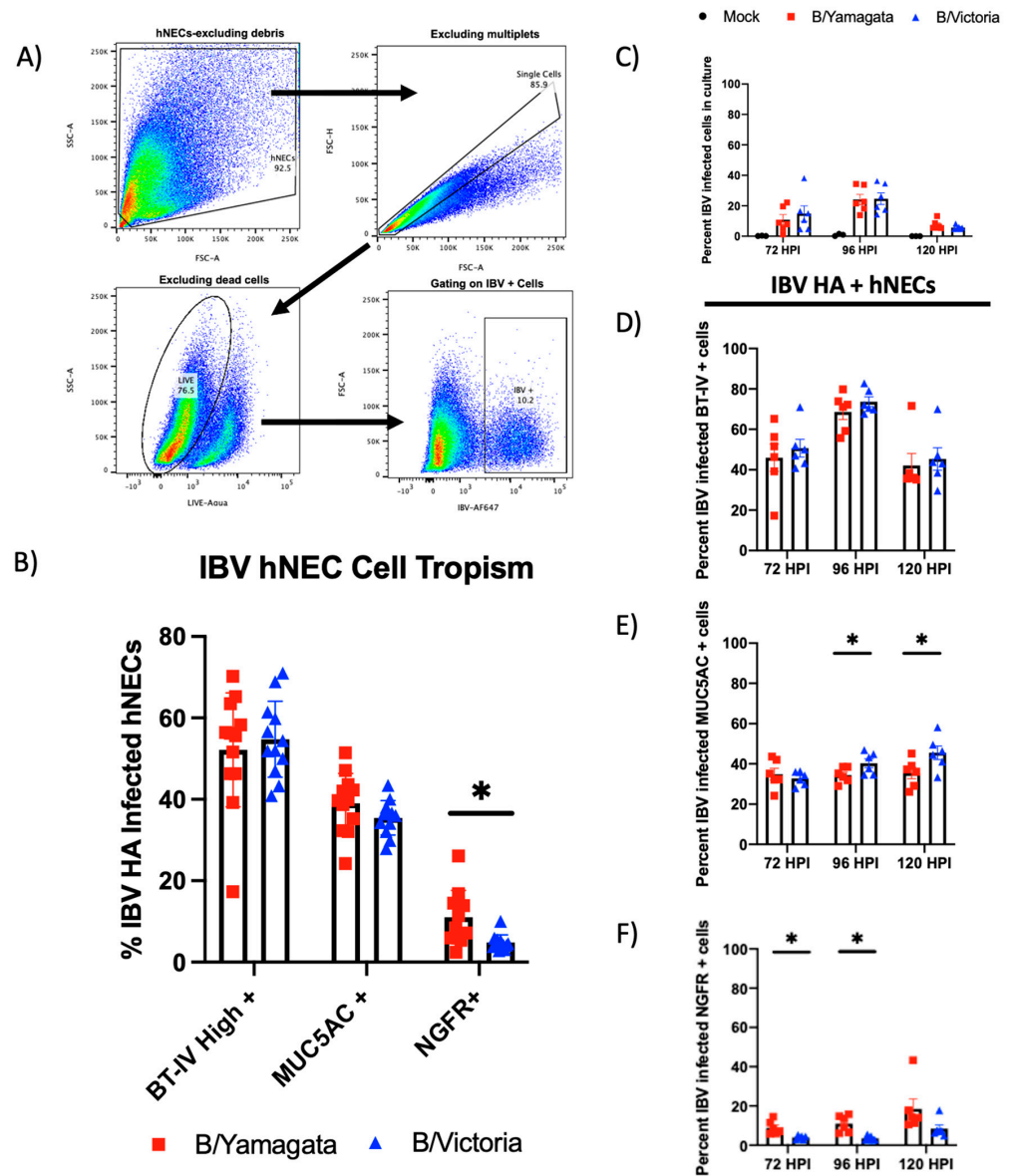
Figure 4. Cell tropism assessment of IBV infection of human nasal cells. (**A**) Gating strategy of assessing IBV-infected hNECs using flow cytometry. Cells were gated by removing debris, single cells, live cells and IBV HA$^+$. (**B**) Additional markers of human nasal cells were used to assess cell tropism including BT-IV as a marker of mature ciliated cells, MUC5AC as a marker of mucin-producing cells and NGFR(CD271) as a marker of respiratory basal cells. Statistical Analysis: Percentages of IBV-infected hNECs were statistically compared between two groups using multiple t-tests. Data represent 72 h infection data from two independent runs with three replicates of each virus and two clinical isolates represented within each lineage. Data points shown in the figure represent combined data from two experiments. (**C**–**F**) Time course of IBV infection in human nasal epithelial cells. IBV-infected hNECs were identified using HA monoclonal antibodies for IBV HA. The specific cell types infected over the course of infection were identified using antibodies specific for the same cellular targets as shown in panel B. (**C**) Percent of IBV-infected cells over infection course. (**D**) Percent of IBV-infected ciliated cells infected over 120 h. (**E**) Percent of IBV-infected MUC5AC + cells over 120 h. (**F**) Percent of IBV-infected NGFR+ cells over 120 h. Cell populations were identified with the following gating strategy: excluding debris, single cells, live cells, IBV + cells, specific cellular stain as described. Three replicate wells were completed for this experiment. Data from two clinical isolates included per lineage. Statistical analysis: Percentages of IBV-infected hNECs were statistically compared between two groups using multiple *t*-tests. * = *p* < 0.05.

3.6. IBV Infected Ciliated Cells Peak at 96 hpi Where Infected Basal and Mucus Producing Cells Continue to Increase through the Course of Infection

We know from our replication kinetics experiments that infectious virion production of influenza B viruses peaks at 72 hpi (Figure 2A). In contrast to our infectious virion production experiments, when we evaluated the number of infected cells over time we saw an increase that peaked at 96 hpi prior to decrease (Figure 4C), with approximately 20% of the total cells infected at that time. The infected ciliated cells drive this pattern as the most infected cell type with peak number of infected cells at 96 hpi (Figure 4D). In contrast to the ciliated cells, IBV-infected MUC5AC-producing cells continue to increase throughout the course of acute infection (Figure 4E). This pattern was consistent with what was noted in infected basal cells. The previously noted pattern of increased IBV basal cell infection in B/Yamagata-infected cultures was again seen at 96 hpi but was not statistically significant at 120 hpi (Figure 4F).

3.7. Pro-Inflammatory Cytokine and Chemokine Production Induced by Influenza B Infection Was Predominantly Defined by IL-6, G-CSF, MCP-1 and TGF-a

To expand the understanding of innate immune responses in influenza B virus infection using protein level immunoassays, a custom Luminex panel was designed to detect commonly upregulated cytokines and chemokines in response to infection with influenza and other respiratory viruses [32]. Cytokine and chemokine production was evaluated both at 48 hpi and 96 hpi. Cytokine production is about 4-fold higher at 96 hpi compared with the 48 h time point (Figure 5A,B). Regardless of significantly greater production, relationships of cytokines and chemokines produced remained relatively similar between time points. CXCL-10, IL-6, G-CSF, MCP-1, TGF-a, TNF-a, MIP-2-A, BAFF, MDC, TRAIL-R2 and MIP-1-A all had at least 2-fold change from mock-infected wells, although many proteins in the panel showed some degree of upregulation post-infection (Figure 5A,B). CXCL-10 had the highest degree of upregulation between 30- and 50-fold mock at 96 hpi (data not on graph given scale difference). There was no significant difference between cytokine production in response to infection when comparing B/Yamagata and B/Victoria (Supplemental Table S1).

3.8. RNAseq of B/Victoria and B/Yamagata Infected hNECs

To expand on post-infection innate responses, bulk RNAseq was performed to determine the gene expression profiles of B/Victoria and B/Yamagata-infected hNEC cultures at 48 hpi. Using Partek Flow, raw reads were demultiplexed and assigned to samples. The average sequencing quality across all samples measured by Phred was Q36. Sample Jo4_337_1_S36 (Yamagata_337 Replicate 1) was excluded from analysis as 75% of reads belonged to non-unique singletons which mapped to ribosomal RNA at an average coverage depth of 275 (Supplemental Table S5). The remaining samples averaged a sequencing coverage depth of 71.8 across treatment groups. All included samples resulted in high mapping percent alignment to human genome hg38 at an average of 92.2% (Supplemental Table S6). Hierarchical clustering of rlog transformed count tables indicated strong clustering between samples at the lineage and virus-specific level (Supplemental Figure S2A). Principle component analysis (PCA) of rlog transformed read counts resulted in strong separation by PC2 between IBV lineages and mock treatment of hNECs with the represented variance of PC1 and PC2 to be 58% and 32%, respectively (Supplemental Figure S2B).
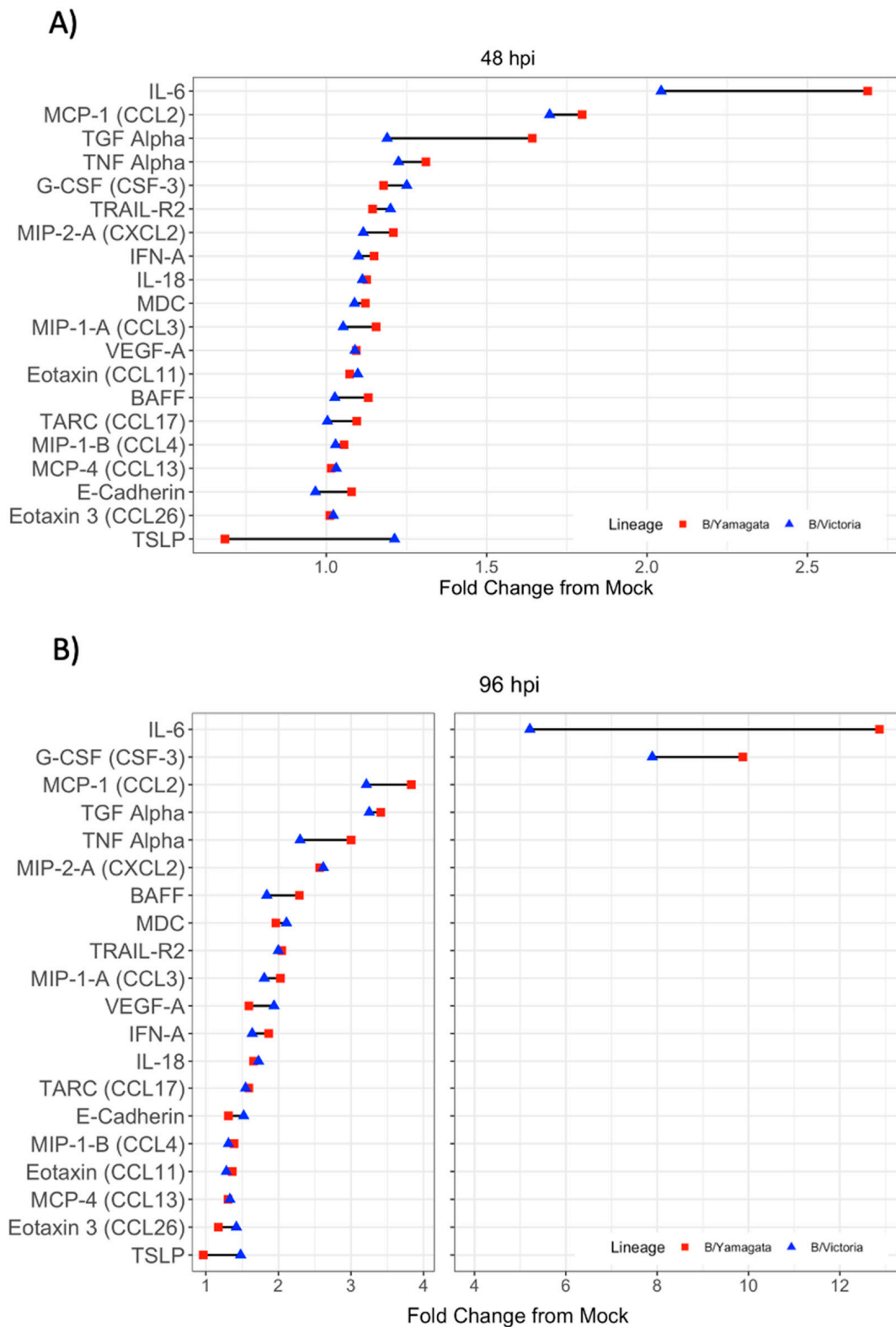
Figure 5. Cytokine expression profiles in the basolateral supernatant of IBV-infected hNEC cultures. (**A**,**B**) General profiles of inflammatory signature of IBV-infected hNECs are shown comparing infections with B/Yamagata and B/Victoria clinical isolates. Data represent two independent experiments. For each experiment, three replicate wells were analyzed. Each IBV lineage combines data from two clinical isolates. There were no statistically significant differences between cytokine profiles following infection between B/Yamagata and B/Victoria.

3.9. Differentially Expressed Gene (DEG) Analysis Identifies Strong Upregulation of Type I and III Interferon Stimulated Gene Families

As all viruses chosen within each lineage belong to identical clades, we chose to focus our DEG analysis by lineage to identify major trends across B/Victoria and B/Yamagata infections. We compared DEGs post-B/Victoria and B/Yamagata infection against mock using DEseq2. Assessment of global transcription across treatment groups revealed distinct profiles in the top 112 DEGs with an adjusted p-value ≤ 0.05 without fold change filtering. Z-scores from rlog-normalized gene counts represent relative expression (Figure 6A). Hierarchal clustering by genes and individual virus expression patterns resulted in distinct clustering by both virus and lineage across all DEGs. Further filtering by both adjusted p-value ≤ 0.05 and a log2 fold change ≥ 1.5 revealed that many top upregulated genes belong to the interferon stimulated gene family and are more highly expressed in B/Victoria infected hNECs (Figure 6B). Differentially expressed genes were further assessed by a log2 fold change ≥ 0.8 and padj ≤ 0.05. A total of 115 genes were upregulated in B/Victoria infected hNECs as compared to mock, whereas only 54 upregulated DEGs were identified in B/Yamagata infections at this threshold (Figure 6A). In total, 53 upregulated genes were shared between the two lineages with 40 of these genes expressed greater in B/Victoria infections (Figure 6B). CXCL10 and ZPB1 were among the top five DEGs in both lineage infections. The remaining genes comprised of interferon and interferon stimulated genes (ISGs) in both B/Victoria and B/Yamagata. IFN lambdas (IFNL1, IFNL2, IFNL3) were among the top upregulated genes in both lineages along with ISGs belonging to the IFIT, IFITM and OAS family including IFI27, IFTM1, IFI6, OAS2 and OAS3 (Figure 7B–F), all of which were expressed greater in B/Victoria. However, IFNL1-3 transcripts do not show significant adjusted p-values, but do show significance in unadjusted p-values (p = 0.000494176, 0.008746909, 0.005584909 for 1–3, respectively) using DESeq2. Receptor transcripts for Type 1 and III interferons do not show significant differences between B/Victoria and B/Yamagata infections but are upregulated in each infection compared to mock (Supplemental Table S1). No upregulation of type I interferon genes for alpha or beta could be detected at 48 hpi. Shared genes upregulated with a higher log2 fold change in B/Victoria infection included known anti-viral proteins IFIT1-3, IFITM1, MX2, IFI44L and ISG15 along with mitochondrial-related gene CMPK2. Implicated ISG15 E3 ligase, HERC6, was also highly upregulated in B/Victoria along with HERC5 and TRIM31 [33]. In total, 49 out of 115 genes were uniquely upregulated in B/Victoria compared to all treatment groups, including CXCL11, IFITM2, EIF2AK2, HLA-B along with many long non-coding RNAs. Only one DEG was identified to be unique in B/Yamagata infection, ENSG00000204745, which is an anaphase-the promoting complex subunit (ANAPC1) pseudogene. Using the adjusted p-value, no downregulated DEGs were shared between B/Victoria- and B/Yamagata-infected hNECs (Figure 7C). Few downregulated genes were identified in B/Victoria infections. COL12A1, a collagen type XIII factor, was downregulated in both B/Victoria infections relative to mock along with ENSG00000274944, a novel unnamed protein. No DEGs were identified as being unique in B/Yamagata infection.

3.10. Gene Ontology Analysis

To further identify differentially expressed gene pathways of infected hNECs, we performed gene ontology analysis on identified DEGs. Only upregulated genes were considered. Analysis was performed on each DEG analysis for all DESeq2 comparison groups by lineage. First, gene set enrichment analysis (GSEA) was performed on DESeq2 output across all comparison groups: B/Victoria vs. mock, B/Yamagata vs. mock and B/Victoria vs. B/Yamagata. We focused on a broader range of genes filtering for a log2 fold change ≥ 0.8 and p-value ≤ 0.5 to evaluate pathways. No unique pathway differences were identified between lineage treatment groups belonging to the antiviral response systems, cytokine signaling type I, type III interferon pathways, and negative regulation of viral replication or processes (Figure 8). B/Victoria vs. mock groups consistently identified a higher number of genes in each shared pathway belonging to cellular response and to type

I interferon, as well as the defense response to virus, type I interferon signaling pathway and negative regulation of viral processes driven by the unique subset of genes upregulated by B/Victoria infection.
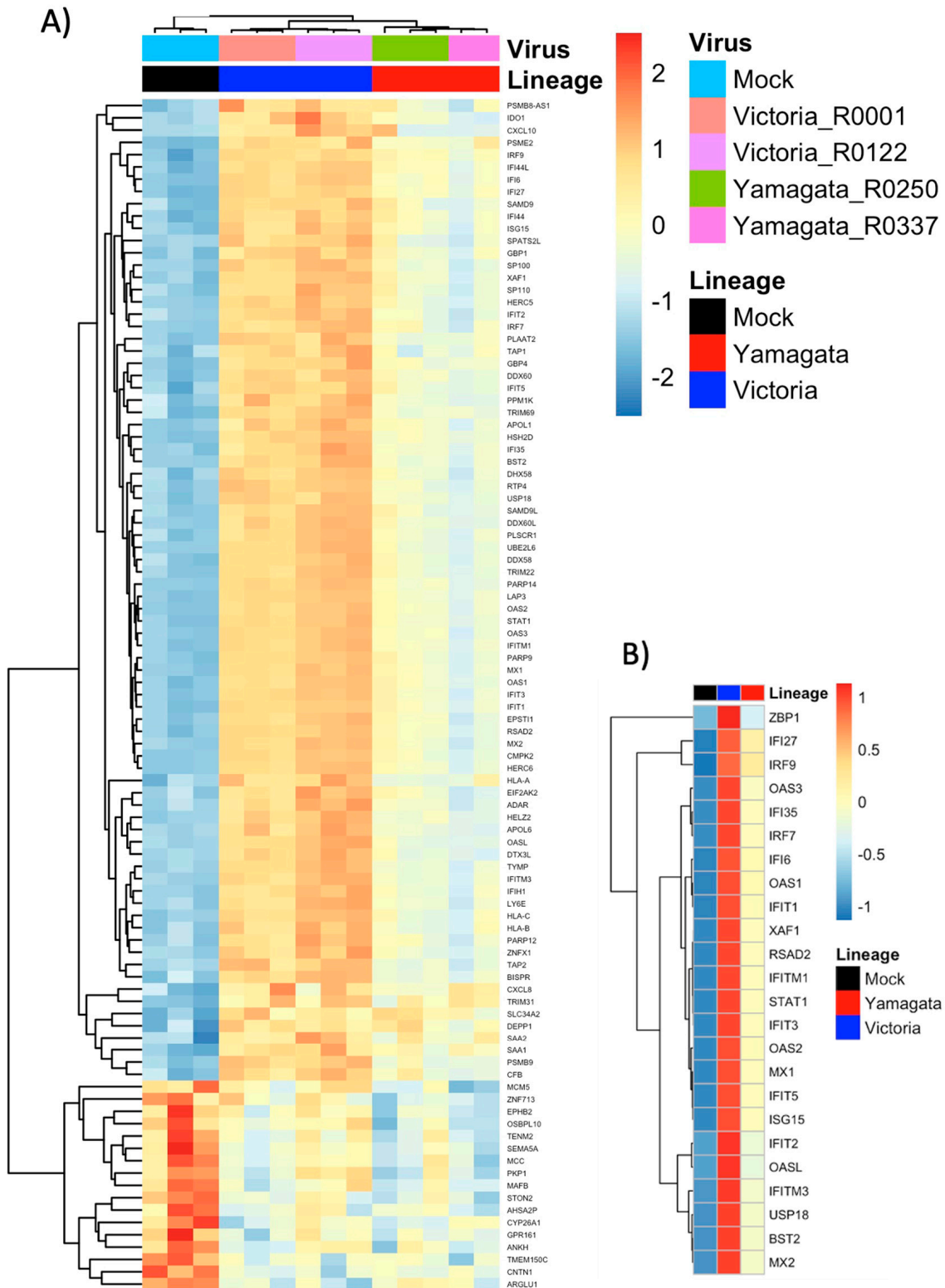
Figure 6. hNEC transcriptional response to B/Victoria and B/Yamagata infection. (**A**) Heatmap of DEGs with a padj $\leq$ 0.05 in hNECs (*n* = 122). (**B**) Subset the complete heatmap of annotated by the top 24 differentially expressed genes summarized by B/Yamagata and B/Victoria lineages.
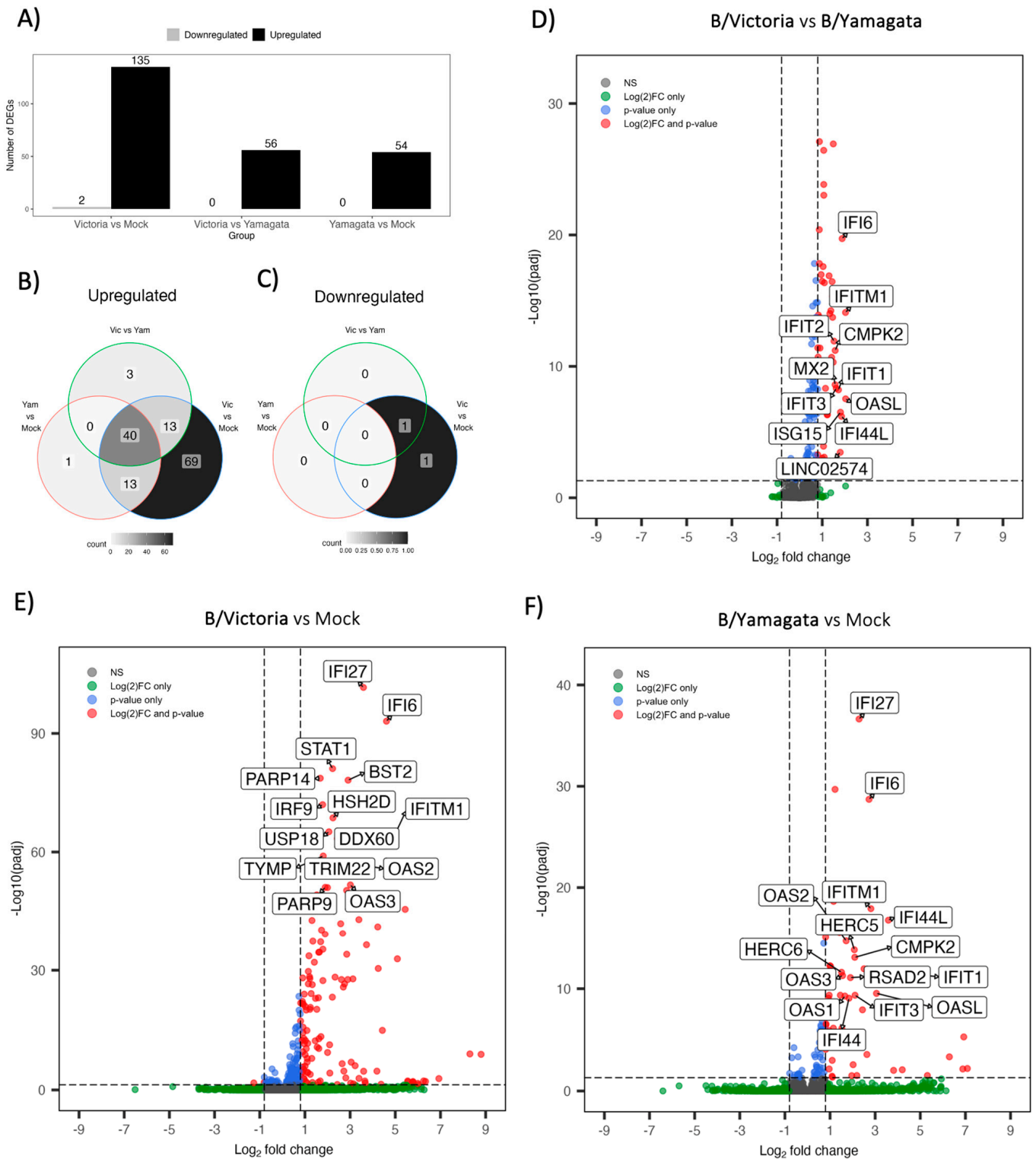
Figure 7. Differentially expressed genes between B/Victoria and B/Yamagata-infected hNECs. Total Differentially expressed genes (DEGs) at threshold cutoffs of a log2 fold change ≥ 0.8 and padj ≤ 0.05. (**A**) Total up and downregulated genes at threshold cutoffs representative of all DE-Seq2 design comparisons. Venn diagrams for each design comparison separated by up (**B**) and down (**C**) regulated genes. Volcano plots of DEGs at threshold for B/Victoria vs. B/Yamagata, (**D**) B/Victoria vs. mock (**E**) and Yamagata vs. mock (**F**).
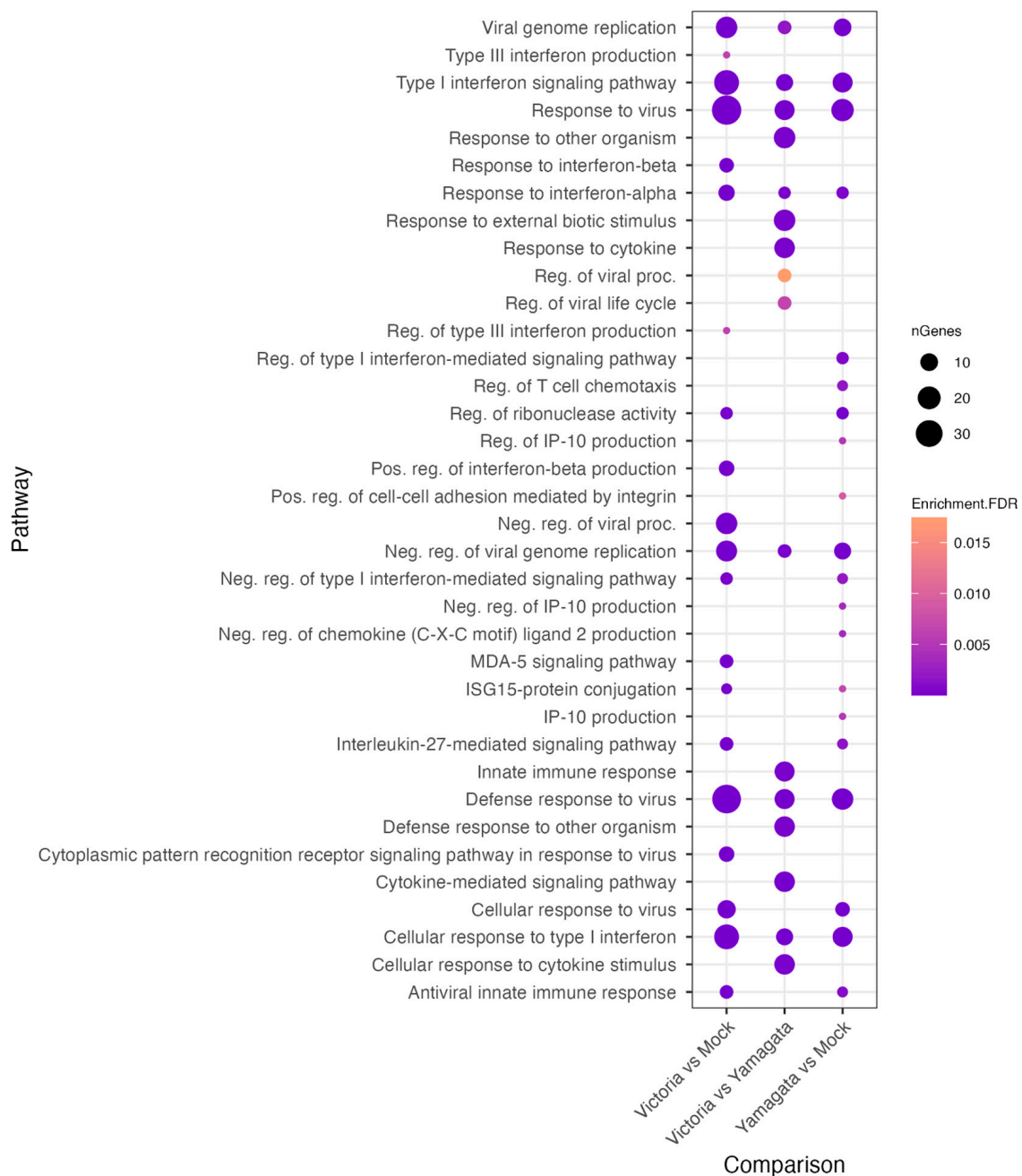
Figure 8. Pathways differentially regulated during B/Victoria and B/Yamgata infection. Pathway enrichment plot representing the top enriched pathways across all lineage comparison using DEseq2 with threshold cutoffs of padj $\leq$ 0.05 and log2 fold change $\geq$ 0.8 using gprofiler.

3.11. mRNA and Protein Expression of RNAseq Targets

To validate mRNA differential expression from RNAseq, 48 hpi hNEC infections were repeated as described above. Cell lysates were subjected to RT-qPCR and Western blotting for identified upregulated genes in the interferon response gene and antiviral pathways. Total mRNA for ifitm1, zpb1 and oasl were induced after viral infection from both lineages representing results consistent with RNAseq data (Figure 9A,B). For protein production validation, ISGs IFIT2 and IFIT3 were selected and quantified with Western blotting. Induction of IFIT2 and IFIT3 were observed in hNECs across both lineage infection groups with the strongest signal observed in B/Yamagata-infected cells for IFIT2 with similar amounts of protein detected across all virus infections for IFIT3 (Figure 9C).
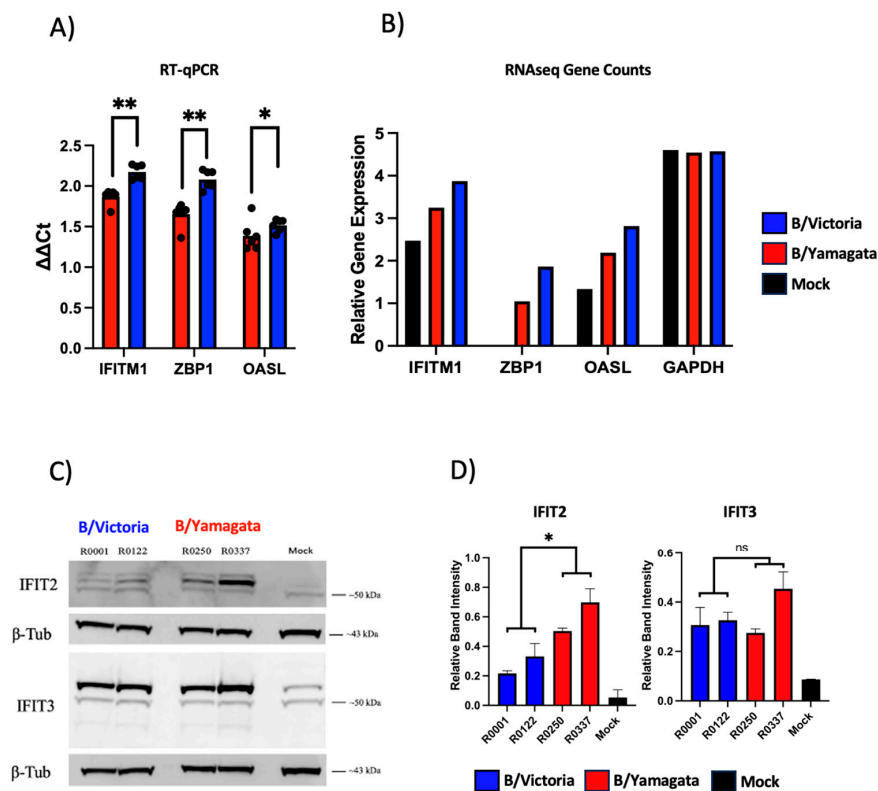
Figure 9. RNAseq validation by RT-qPCR and Western blot. (**A**) RNAseq validating using RT-qPCR of 5 targets: OASL, IFITM1, RBFOX3, USP17L1 and ZBP1. Change in gene expression was calculated using the $2^{-(\Delta\Delta Ct)}$ method and summarized by lineage. Comparisons were performed by two-tailed t-test using Graphpad Prism. (**B**) Relative gene expression counts for each validated gene from rlog normalized RNAseq counts. (**C**) Western blot and relative band intensities of (**D**) IFIT2 and IFIT3 for each virus by lineage from two independent experiments. Statistical significance of normalized band intensities were calculated on GraphPad Prism using a two-way ANOVA and Tukey's multiple comparisons. * = $p < 0.05$ and ** = $p < 0.01$.

3.12. IBV NS1 Sequence Analysis

Given that the pathways that were differentially upregulated between lineages belonged to the interferon and antiviral-related responses, we sought to compare IBV genomes focusing on a known IBV antagonist of these pathways. IBV NS1 is known to be a critical factor for efficient viral replication by inhibition of the host interferon response, including, but not limited, to its ability to bind interferon transcription factors such as IRF-3 along with ISG15 such as ISG15 and IFIT2 [34–36]. Furthermore, genomic analysis of all IBV segments has previously shown that segment 8 encoding NS1 is under greater selection pressure than other segments measured by nonsynonymous to synonymous substitutions for both Yamagata and Victoria [15]. We chose to explore phylogenetic differences in NS1 for B/Yamagata and B/Victoria. To evaluate NS1 protein diversity, 254 NS1 protein sequences were accessed from GISAID belonging to both B/Victoria (*n* = 142) and B/Yamagata (*n* = 108) lineages and aligned to the four viruses used in this study. Phylogenetic analysis of IBV NS1 by maximum likelihood tree construction of the NS1 protein revealed high divergence between the lineages (Figure 10A). The intra-lineage divergence between viruses used in this study shows a higher distance between the B/Yamagata viruses compared to the B/Victoria. Analysis of all NS1 sequences was used to generate consensus sequences for alignments to both lineages along with overall amino acid frequency and richness (Figure 10B). Specific amino acids from consensus sequences were unique by lineage. These include an N-terminal asparagine insertion at position 3 observed exclusively in all B/Victoria viruses. The linker region contained additional regions unique by consensus observed at positions

4, 7, 111, 115, 118, 120, 127 and 139. Calculating Shannon entropy by alignment site revealed the highest amount of NS1 variation to be at the N-terminal alignment positions 3 and 4 and residues within the linker region from 110 to 140 (Figure 10B). The C-terminal region contained fewer variable residues with a notable K177R B/Victoria to B/Yamagata consensus lineage difference. The remaining entropy belonged to intra-lineage variation.
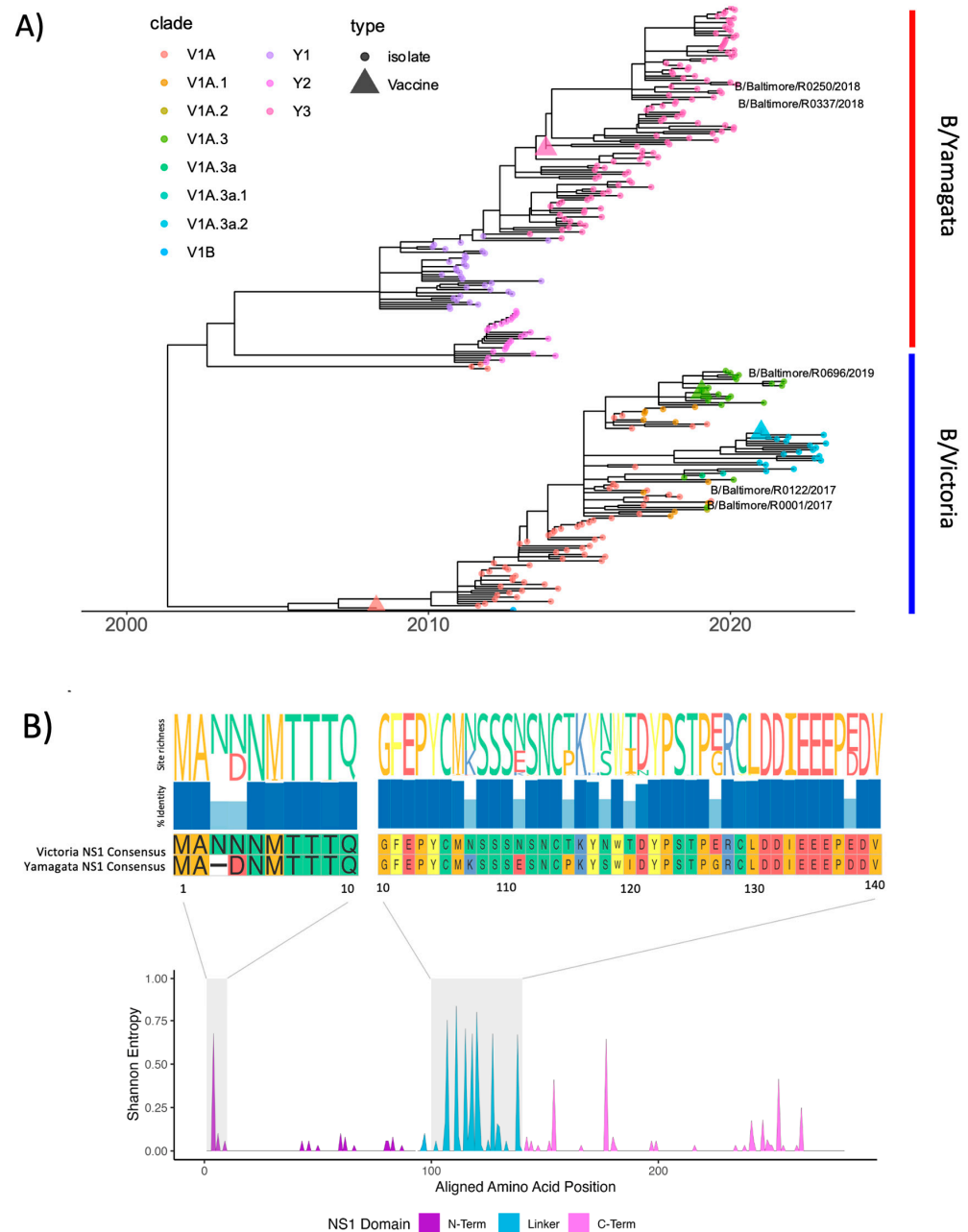
Figure 10. Influenza B NS1 protein has diverged by lineage and HA clade (**A**) influenza B phylogenetic tree of representative NS1 sequences (*n* = 283) isolated between 2009 and 2023. NS1 open reading frames were extracted using the NCBI influenza annotation tool (https://www.ncbi.nlm.nih.gov/genomes/FLU/annotation/ (accessed on 14 March 2023)) and aligned using Muscle (v3.8.31) with the PPP algorithm. Time-scaled maximum-likelihood trees were constructed using treetime v0.9.6 and annotated by lineage in R (v4.1.2) using ggtree v3.16. (**B**) Amino acid alignments were used to calculate Shannon entropy by site using the vegan v2.6-4 and seqinr 4.2-23 packages and visualized using R v4.1.1. IBV NS1 domains were annotated according to PDB: 5DIL and BMRB: 25462. Amino acid site richness and percent identity were visualized using ggmsa 3.16.

4. Discussion

IBV has been given less research attention compared to IAV, likely due to a smaller proportion of annual infections and decreased pandemic potential due to the lack of diverse animal reservoirs [37]. IBV historically has accounted for approximately one-quarter of the influenza infections and has a major impact on the pediatric population, especially during antigenic drift years [5]. The landscape of IBV amidst the SARS-CoV-2 pandemic has drastically changed. The B/Victoria lineage circulation decreased; however, increased genetic diversity was seen leading to a vaccine change in the northern hemisphere in 2021. B/Yamagata has not been sequenced since March 2020. Although many hypothesize that this lineage may be extinct, IBV has historically seen pauses like this in circulation; therefore, more surveillance is needed to fully assess B/Yamagata's disappearance [14]. The primary purpose of this study was to compare the acute, in vitro respiratory epithelial infection and immune response to IBV infections as a whole and further to compare the two lineages of IBV. The representative viruses used to evaluate these lineages were chosen from the years 2016–2019, notably a time of increased diversity for B/Victoria and limited diversity in B/Yamagata. The individual analyses for viral characterization were completed with viruses of each lineage of the same clade. It would be equally beneficial to perform a more extensive analysis of a broader panel of viruses isolated across a wider range of time to see the changes in in vitro replication that accrue over time within and across lineages.

Lau et al. recently evaluated hemagglutinin inhibition (HAI) titers comparing B/Yamagata and B/Victoria in IBVs isolated from 2009 to 2014. They found that in adults, B/Yamagata viruses lead to higher antibody responses to vaccination. To evaluate this using a different method, we used serum neutralization antibody assays [38], with our findings being consistent with Lau et al. in a higher mean post-vaccination antibody response in B/Yamagata compared to B/Victoria. We hypothesize that this could be due to antigenic imprinting given that B/Yamagata clade 3 has dominated as a circulating clade since 2012, whereas recent B/Victoria genetic diversity has given rise to a new dominating clade roughly every two years since 2015. Our findings of differences between the vaccine and circulating strains are not surprising given the known drift of B/Victoria in the 2019 season and the accumulation of egg adaption mutations at antigenic sites of IBV vaccine strains [39].

In the 2016–2018 seasons, B/Yamagata clade 3 viruses dominated and B/Victoria V1A.1 circulation was diminished in favor of the alternate lineage (Figure 1A). We assessed replication efficiency and peak infection using replication growth curves between these viruses, finding similar onset of infection and burst size. We conclude that innate viral replication factors likely do not play a role in the pattern of shifting dominance between these viruses in circulation and rather likely are due to patterns of immune memory in the population, as has been studied by several groups [40,41]. Our plaque evaluation between these lineages showed an increased plaque size with B/Yamagata viruses suggesting that there are some innate viral factors making these lineages distinct. To better understand the ever-changing variation in fitness and antigenicity in IBV, we need regular assessments of circulating viruses as well as assessment of human immune response to novel viruses.

We set out to understand the initial 5-day course of infection in the nasal respiratory epithelium beyond replication kinetics. Bui et al. showed that IBV infects multiple cell types at 37 °C in the bronchial epithelium [42]. We chose to take a quantitative approach to the nasal epithelium using low MOI hNEC infections and analyzing infected cell numbers using flow cytometry. Our data agree with Bui et al. and add to this knowledge by highlighting the changing dynamic of the infected nasal epithelial subsets during acute infection. At the peak of infection (72 hpi), most infected cells are ciliated cells, followed by mucus-producing cells and then basal cells. There was a statistically significant increase in basal cell infection with B/Yamagata compared to B/Victoria, whereas other infected cell type percentages were not different. As we showed a variation in plaque size as well in B/Yamgata, we hypothesize that this may suggest that cell to cell virion spread may be more efficient in the B/Yamagata lineage without a significant change in total virion

production. We showed that although virion production peaks at 72 hpi, the number of infected cells peaks at 96 hpi. This pattern is driven by the infection of ciliated cells with the mucus-producing cells and the basal cell populations following a different pattern of increasing throughout the course of infection. This is likely secondary to IBV infection-mediated cell death of the ciliated cells in early infection, leading to increased exposure and therefore vulnerability of other cell types in late infection.

A broadly descriptive phenotype of the immune response to IBV infection, to our knowledge, has not been reported. We chose to evaluate hNEC culture responses to infection using both protein immunoassays as well as bulk RNAseq. Protein immunoassays were notable for significant upregulation of CXCL-10, IL-6, G-CSF, MCP-1 and TGF-α. There was no significant difference between lineages in any chemokine or cytokine that was measured in our analysis. Additionally, a study in IAV showed similar upregulation patterns [40]. This suggests that with these specific protein analytes, there is no variation in immune response between lineages, and these upregulated chemokines and cytokines may show a similar pattern to influenza A, although this was not directly evaluated.

To our knowledge, our study is the first to employ distinct RNAseq characterization of the hNECs infected with IBV at the lineage level. At 48 hpi, we observe a large number of upregulated DEGs belonging to the interferon and antiviral pathways, including interferon-stimulated genes (ISGs). Curiously, there is no detectable level of type I interferon (alpha or beta) transcripts in the RNAseq dataset while interferon lambda (1–3) is highly upregulated in both infections. At 48 hpi, we speculate that the dominant interferon response has switched primarily to the type III response away from the production of acute-onset type I interferon, which is common at many mucosal barrier surfaces. Protein measurement of type I interferon by Luminex shows a minimal and equal increase from mock treatment, reaching only 1.5-old induction for both B/Victoria and B/Yamagata infections. This is not surprising given that hNECs do not produce high levels of type I interferon [43]. Upregulation of OAS, IFIT and IFITM gene families in all IBV infections aligns with previously cited studies performed in immortalized cell lines, suggesting that these pathways are critical in the innate immune defense against IBV. Also consistent with previous reports from nasal swab assessment, we saw robust CXCL10 (Supplemental Table S3) expression across both B/Victoria and B/Yamagata [44]. Our findings alongside others identify OAS, interferon response, and CXCL10 as critical to innate immune defense against IBV.

While both lineages share many genes belonging to the ISG response, RNAseq reveals that B/Victoria transcriptional responses are higher in both the multitude and magnitude of ISGs as well as uniquely upregulating genes such as CXCL11, IFITM2 and STAT2 compared to B/Yamagata infections. ISGs IFIT2 and IFIT3 were strongly expressed in both lineage infections as verified using Western blotting. However, amounts of IFIT2 and IFIT3 appear to be slightly higher in B/Yamagata infections with an exceptionally strong band in B/Baltimore/R0337/2018 infection. The importance of these proteins during influenza infection is well demonstrated with evidence of a dual pro-viral function to bias viral transcript production in both IBV and IAV in vitro infections [2,7]. Although these differences are minor, these findings suggest that the way that IBV lineages interact with immune response may vary between lineages. ISG15 ubiquitin-like protein transcripts are upregulated in both lineage treatments with stronger transcript abundance measured in B/Victoria infected hNECs. Several studies have demonstrated that this protein is important for viral replication control in vitro [45,46].

We hypothesize the lineage-specific variation that we show in the innate immune response to IBV to be from the divergence in NS1 sequences over time. Functionally, the influenza NS1 proteins are well known to bind key players in the interferon response at the transcriptional, translational and post-translational levels. However, the IBV NS1 encodes for additional RNA-binding residues in the N-terminal domain which allows for unique binding specificity to host antiviral proteins such as ISG15 compared to IAV [11,35,46,47]. Furthermore, IBV NS1 sequence homology with the IAV NS1 is less than 25%, preventing successful sequence comparisons to known functional assays across the viruses. A compre-

hensive genome analysis by Virk et al., 2019 highlights the continued diversification across all genome segments of both the Victoria and Yamagata lineages consistent with a strict molecular clock model [15,48]. Our analysis recapitulates lineage-specific divergence of the IBV NS1 protein, which is consistent with HA and NA diversification. However, metrics to identify selection such as the ratio of nonsynonymous to synonymous polymorphisms (dN/dS) have identified that NS undergoes higher levels of positive selections compared to every other segment in both lineages. While not indicative of function, this metric identifies NS as a strong contributor to the evolution of influenza B viruses. Furthermore, the influenza B genome is not known to encode supplemental proteins with primary interferon-suppressing functions such as the influenza A PB1-F2, making NS1 a strong candidate for differential regulation [49].

In summary, we set out to describe in detail the in vitro properties of IBV lineages and the hNEC response to infection with the two lineages of IBV, B/Yamagata and B/Victoria [11,35,46,47]. Our findings of equivalent infectious virus production between lineages, despite significant differences in the transcriptomic profiles, indicate there are differences between the lineages outside of antigenic differences in the HA protein.

Supplementary Materials: The following supporting information can be downloaded at: https://www.mdpi.com/article/10.3390/v15091956/s1. Supplemental Figure S1. Identification of hNEC subpopulations by flow cytometry. (A) FlowJo Plots to show gating of hNEC subpopulations. BT-IV high cells were gated using SSC-A as it facilitated appropriate gating to increased granularity of ciliated cells. Other cell types were gated using histograms, fluorescent spread shown. (B) BT-IV-AF488 versus NGFR-PE shows a lack of co-staining consistent with population identities. (C). BT-IV –AF488 versus MUC5AC-BV605 shows MUC5AC is ciliated and non-ciliated cells. (D) MUC5AC-BV605 versus NGFR-PE shows a lack of co-staining consistent with population identities. Supplemental Figure S2 Normalized gene count data generated through Partek Flow 'quantify to annotation model' normalized using rlog. (B) Distance matrices calculated from normalized count data. PCA of normalized count data. Supplemental Table S1: Annotated DESeq2 results for differential gene expression by lineage. Supplemental Table S2: Gene Ontology analysis of differentially expressed gene. Supplemental Table S3: Raw data MagPix Cytokine panel output with standard curves and analysis of geometric means. Supplemental Table S4: GISIAD isolate IDs and metadata for all sequences analyzed in this study. Supplemental Table S5: Post-alignment quality control tables from RNAseq experiments and Supplemental Table S6 annotations.

Institutional Review Board Statement: IBV Clinical Isolate Collection: The human subjects' protocol was approved by the Johns Hopkins School of Medicine Institutional Review Board (IRB90001667) and the National Institutes of Health Division of Microbiology and Infectious Diseases (protocol 15-0103). Neutralizing Antibody Assays: This study was approved by the JHU School of Medicine Institutional Review Board, IRB00288258. Serum samples for this study were obtained from healthcare workers (HCWs) recruited from the Johns Hopkins Centers for Influenza Research and Surveillance (JHCEIRS) during the annual Johns Hopkins Hospital (JHH) employee influenza vaccination campaign. Pre- and post-vaccination (~28 day) human serum were collected from subjects, who provided written informed consent prior to participation.

Informed Consent Statement: Informed consent was obtained from all subjects involved in the study. All human specimen were deidentified before use.

References

1. Uyeki, T.M.; Hui, D.S.; Zambon, M.; Wentworth, D.E.; Monto, A.S. Influenza. *Lancet* **2022**, *400*, 693–706. [CrossRef] [PubMed]
2. CDC. *Burden of Influenza*; Centers for Disease Control and Prevention: Atlanta, GA, USA, 2022.
3. Jackson, D.; Elderfield, R.A.; Barclay, W.S. Molecular Studies of Influenza B Virus in the Reverse Genetics Era. *J. Gen. Virol.* **2011**, *92*, 1–17. [CrossRef] [PubMed]
4. Caini, S.; Huang, Q.S.; Ciblak, M.A.; Kusznierz, G.; Owen, R.; Wangchuk, S.; Henriques, C.M.; Njouom, R.; Fasce, R.A.; Yu, H.; et al. Epidemiological and virological characteristics of influenza B: Results of the Global Influenza B Study. *Influenza Other Respir. Viruses* **2015**, *9* (Suppl. 1), 3–12. [CrossRef] [PubMed]
5. Caini, S.; Kusznierz, G.; Garate, V.V.; Wangchuk, S.; Thapa, B.; de Paula Júnior, F.J.; Ferreira de Almeida, W.A.; Njouom, R.; Fasce, R.A.; Bustos, P.; et al. The Epidemiological Signature of Influenza B Virus and Its B/Victoria and B/Yamagata Lineages in the 21st Century. *PLoS ONE* **2019**, *14*, e0222381. [CrossRef]
6. Su, S.; Chaves, S.S.; Perez, A.; D'Mello, T.; Kirley, P.D.; Yousey-Hindes, K.; Farley, M.M.; Harris, M.; Sharangpani, R.; Lynfield, R.; et al. Comparing Clinical Characteristics between Hospitalized Adults with Laboratory-Confirmed Influenza A and B Virus Infection. *Clin. Infect. Dis.* **2014**, *59*, 252–255. [CrossRef]
7. Dwyer, D.E.; Lynfield, R.; Losso, M.H.; Davey, R.T.; Cozzi-Lepri, A.; Wentworth, D.; Uyeki, T.M.; Gordin, F.; Angus, B.; Qvist, T.; et al. Comparison of the Outcomes of Individuals with Medically Attended Influenza A and B Virus Infections Enrolled in 2 International Cohort Studies over a 6-Year Period: 2009–2015. *Open Forum. Infect. Dis.* **2017**, *4*, ofx212. [CrossRef]
8. Tran, D.; Vaudry, W.; Moore, D.; Bettinger, J.A.; Halperin, S.A.; Scheifele, D.W.; Jadvji, T.; Lee, L.; Mersereau, T. Hospitalization for Influenza A Versus B. *Pediatrics* **2016**, *138*, e20154643. [CrossRef]
9. Centers for Disease Control and Prevention (CDC). Prevention and Control of Seasonal Influenza with Vaccines. Recommendations of the Advisory Committee on Immunization Practices–United States, 2013–2014. *MMWR Recomm. Rep.* **2013**, *62*, 1–43.
10. Kuo, S.M.; Chen, G.W.; Velu, A.B.; Dash, S.; Han, Y.J.; Tsao, K.C.; Shih, S.R. Circulating Pattern and Genomic Characteristics of Influenza B Viruses in Taiwan from 2003 to 2014. *J. Formos. Med. Assoc.* **2016**, *115*, 510–522. [CrossRef]
11. Frey, S.; Vesikari, T.; Szymczakiewicz-Multanowska, A.; Lattanzi, M.; Izu, A.; Groth, N.; Holmes, S. Clinical Efficacy of Cell CultureDerived and Egg-Derived Inactivated Subunit Influenza Vaccines in Healthy Adults. *Clin. Infect. Dis.* **2010**, *51*, 997–1004. [CrossRef]
12. Domachowske, J.B.; Pankow-Culot, H.; Bautista, M.; Feng, Y.; Claeys, C.; Peeters, M.; Innis, B.L.; Jain, V. A Randomized Trial of Candidate Inactivated Quadrivalent Influenza Vaccine versus Trivalent Influenza Vaccines in Children Aged 3–17 Years. *J. Infect. Dis.* **2013**, *207*, 1878–1887. [CrossRef] [PubMed]
13. Reed, C.; Meltzer, M.I.; Finelli, L.; Fiore, A. Public Health Impact of Including Two Lineages of Influenza B in a Quadrivalent Seasonal Influenza Vaccine. *Vaccine* **2012**, *30*, 1993–1998. [CrossRef] [PubMed]
14. Rota, P.A.; Wallis, T.R.; Harmon, M.W.; Rota, J.S.; Kendal, A.P.; Nerome, K. Cocirculation of Two Distinct Evolutionary Lineages of Influenza Type B Virus since 1983. *Virology* **1990**, *175*, 59–68. [CrossRef] [PubMed]
15. Virk, R.K.; Jayakumar, J.; Mendenhall, I.H.; Moorthy, M.; Lam, P.; Linster, M.; Lim, J.; Lin, C.; Oon, L.L.; Lee, H.K.; et al. Divergent Evolutionary Trajectories of Influenza B Viruses Underlie Their Contemporaneous Epidemic Activity. *Proc. Natl. Acad. Sci. USA* **2020**, *117*, 619–628. [CrossRef] [PubMed]
16. Sharabi, S.; Drori, Y.; Micheli, M.; Friedman, N.; Orzitzer, S.; Bassal, R.; Glatman-Freedman, A.; Shohat, T.; Mendelson, E.; Hindiyeh, M.; et al. Epidemiological and Virological Characterization of Influenza B Virus Infections. *PLoS ONE* **2016**, *11*, e0161195. [CrossRef]
17. FluView Interactive | CDC. 2020. Available online: https://www.cdc.gov/flu/weekly/fluviewinteractive.htm (accessed on 3 February 2023).
18. Bian, J.-R.; Nie, W.; Zang, Y.-S.; Fang, Z.; Xiu, Q.-Y.; Xu, X.-X. Clinical Aspects and Cytokine Response in Adults with Seasonal Influenza Infection. *Int. J. Clin. Exp. Med.* **2014**, *7*, 5593–5602.

19. Information for Molecular Diagnosis of Influenza Virus. WHO Protocols for Influenza Virus Detection. 6th Revision. January 2020. Available online: https://cdn.who.int/media/docs/default-source/influenza/molecular-detention-of-influenza-viruses/protocols_influenza_virus_detection_feb_2021.pdf?sfvrsn=df7d268a_5 (accessed on 3 February 2020).

20. Chan, W.M.; Wong, L.H.; So, C.F.; Chen, L.L.; Wu, W.L.; Ip, J.D.; Lam, A.H.Y.; Yip, C.C.; Yuen, K.Y.; To, K.K. Development and Evaluation of a Conventional RT-PCR for Differentiating Emerging Influenza B/Victoria Lineage Viruses with Hemagglutinin Amino Acid Deletion from B/Yamagata Lineage Viruses. *J. Med. Virol.* **2020**, *92*, 382–385. [CrossRef]

21. Reed, L.J.; Muench, H. A simple method of estimating fifty per cent endpoints. *Am. J. Epidemiol.* **1938**, *27*, 493–497. [CrossRef]

22. Elbe, S.; Buckland-Merrett, G. Data, Disease and Diplomacy: GISAID's Innovative Contribution to Global Health. *Glob. Chall.* **2017**, *1*, 33–46. [CrossRef]

23. Yu, G.; Smith, D.K.; Zhu, H.; Guan, Y.; Lam, T.T.-Y. Ggtree: An r Package for Visualization and Annotation of Phylogenetic Trees with Their Covariates and Other Associated Data. *Methods Ecol. Evol.* **2017**, *8*, 28–36. [CrossRef]

24. R Core Team. *R: A Language and Environment for Statistical Computing*; R Foundation for Statistical Computing: Vienna, Austria, 2022.

25. Love, M.I.; Huber, W.; Anders, S. Moderated estimation of fold change and dispersion for RNA-seq data with DESeq2. *Genome Biol.* **2014**, *15*, 1–21. [CrossRef]

26. Reimand, J.; Kolde, R.; Arak, T. *gProfileR: Interface to the "g:Profiler" Toolkit, R package Version 0.6*; University of Tartu: Tartu, Estonia, 2018.

27. Jensen-Smith, H.C.; Ludueña, R.F.; Hallworth, R. Requirement for the βI and βIV Tubulin Isotypes in Mammalian Cilia. *Cell Motil. Cytoskelet.* **2003**, *55*, 213. [CrossRef]

28. Gohy, S.; Carlier, F.M.; Fregimilicka, C.; Detry, B.; Lecocq, M.; Ladjemi, M.Z.; Verleden, S.; Hoton, D.; Weynand, B.; Bouzin, C.; et al. Altered Generation of Ciliated Cells in Chronic Obstructive Pulmonary Disease. *Sci. Rep.* **2019**, *9*, 17963. [CrossRef] [PubMed]

29. Bonser, L.R.; Koh, K.D.; Johansson, K.; Choksi, S.P.; Cheng, D.; Liu, L.; Sun, D.I.; Zlock, L.T.; Eckalbar, W.L.; Finkbeiner, W.E.; et al. Flow-Cytometric Analysis and Purification of Airway Epithelial-Cell Subsets. *Am. J. Respir. Cell Mol. Biol.* **2021**, *64*, 308–317. [CrossRef] [PubMed]

30. Pharo, E.A.; Williams, S.M.; Boyd, V.; Sundaramoorthy, V.; Durr, P.A.; Baker, M.L. HostPathogen Responses to Pandemic Influenza H1N1pdm09 in a Human Respiratory Airway Model. *Viruses* **2020**, *12*, 679. [CrossRef] [PubMed]

31. Ruiz García, S.; Deprez, M.; Lebrigand, K.; Cavard, A.; Paquet, A.; Arguel, M.J.; Magnone, V.; Truchi, M.; Caballero, I.; Leroy, S.; et al. Novel Dynamics of Human Mucociliary Differentiation Revealed by Single-Cell RNA Sequencing of Nasal Epithelial Cultures. *Development* **2019**, *146*, dev177428. [CrossRef] [PubMed]

32. Betakova, T.; Kostrabova, A.; Lachova, V.; Turianova, L. Cytokines Induced during Influenza Virus Infection. *Curr. Pharm. Des.* **2017**, *23*, 2616–2622. [CrossRef]

33. Oudshoorn, D.; van Boheemen, S.; Sánchez-Aparicio, M.T.; Rajsbaum, R.; García-Sastre, A.; Versteeg, G.A. HERC6 Is the Main E3 Ligase for Global ISG15 Conjugation in Mouse Cells. *PLoS ONE* **2012**, *7*, e29870. [CrossRef]

34. Tran, V.; Ledwith, M.P.; Thamamongood, T.; Higgins, C.A.; Tripathi, S.; Chang, M.W.; Benner, C.; García-Sastre, A.; Schwemmle, M.; Boon, A.C.; et al. Influenza Virus Repurposes the Antiviral Protein IFIT2 to Promote Translation of Viral mRNAs. *Nat. Microbiol.* **2020**, *5*, 1490–1503. [CrossRef]

35. Zhao, C.; Sridharan, H.; Chen, R.; Baker, D.P.; Wang, S.; Krug, R.M. Influenza B Virus Non-Structural Protein 1 Counteracts ISG15 Antiviral Activity by Sequestering ISGylated Viral Proteins. *Nat. Commun.* **2016**, *7*, 12754. [CrossRef]

36. Donelan, N.R.; Dauber, B.; Wang, X.; Basler, C.F.; Wolff, T.; García-Sastre, A. The N- and C-Terminal Domains of the NS1 Protein of Influenza B Virus Can Independently Inhibit IRF-3 and Beta Interferon Promoter Activation. *J. Virol.* **2004**, *78*, 11574. [CrossRef] [PubMed]

37. Osterhaus, A.D.M.E.; Rimmelzwaan, G.F.; Martina, B.E.E.; Bestebroer, T.M.; Fouchier, R.A.M. Influenza B Virus in Seals. *Science* **2000**, *288*, 1051–1053. [CrossRef] [PubMed]

38. Lau, Y.C.; Perera, R.A.; Fang, V.J.; Luk, L.H.; Chu, D.K.; Wu, P.; Barr, I.G.; Peiris, J.M.; Cowling, B.J. Variation by Lineage in Serum Antibody Responses to Influenza B Virus Infections. *PLoS ONE* **2020**, *15*, e0241693. [CrossRef] [PubMed]

39. Wilson, J.L.; Zhou, R.; Liu, H.; Rothman, R.; Fenstermacher, K.Z.; Pekosz, A. Antigenic alteration of 2017-2018 season influenza B vaccine by egg-culture adaption. *Front. Virol.* **2022**, *2*, 933440. [CrossRef]

40. Laurie, K.L.; Horman, W.; Carolan, L.A.; Chan, K.F.; Layton, D.; Bean, A.; Vijaykrishna, D.; Reading, P.C.; McCaw, J.M.; Barr, I.G. Evidence for Viral Interference and Cross-reactive Protective Immunity between Influenza B Virus Lineages. *J. Infect. Dis.* **2018**, *217*, 548–559. [CrossRef] [PubMed]

41. van de Sandt, C.E.; Dou, Y.; Vogelzang-van Trierum, S.E.; Westgeest, K.B.; Pronk, M.R.; Osterhaus, A.D.; Fouchier, R.A.; Rimmelzwaan, G.F.; Hillaire, M.L. Influenza B Virus-Specific CD8+ T-lymphocytes Strongly Cross-React with Viruses of the Opposing Influenza B Lineage. *J. Gen. Virol.* **2015**, *96*, 2061–2073. [CrossRef]

42. Bui, C.H.; Chan, R.W.; Ng, M.M.; Cheung, M.C.; Ng, K.C.; Chan, M.P.; Chan, L.L.; Fong, J.H.; Nicholls, J.M.; Peiris, J.M.; et al. Tropism of Influenza B Viruses in Human Respiratory Tract Explants and Airway Organoids. *Eur. Respir. J.* **2019**, *54*, 1900008. [CrossRef]

43. Ali, S.; Mann-Nüttel, R.; Schulze, A.; Richter, L.; Alferink, J.; Scheu, S. Sources of type I interferons in infectious immunity: Plasmacytoid dendritic cells not always in the driver's seat. *Front. Immunol.* **2019**, *10*, 422559. [CrossRef]

44. Dissanayake, T.K.; Schäuble, S.; Mirhakkak, M.H.; Wu, W.L.; Ng, A.C.K.; Yip, C.C.; López, A.G.; Wolf, T.; Yeung, M.L.; Chan, K.H.; et al. Comparative Transcriptomic Analysis of Rhinovirus and Influenza Virus Infection. *Front. Microbiol.* **2020**, *11*, 1580. [CrossRef]

45. Perng, Y.-C.; Lenschow, D.J. ISG15 in Antiviral Immunity and Beyond. *Nat. Rev. Microbiol.* **2018**, *16*, 423–439. [CrossRef]

46. Guan, R.; Ma, L.C.; Leonard, P.G.; Amer, B.R.; Sridharan, H.; Zhao, C.; Krug, R.M.; Montelione, G.T. Structural basis for the sequence-specific recognition of human ISG15 by the NS1 protein of influenza B virus. *Proc. Natl. Acad. Sci. USA* **2011**, *108*, 13468–13473. [CrossRef] [PubMed]

47. Yuan, W.; Krug, R.M. Influenza B Virus NS1 Protein Inhibits Conjugation of the Interferon (IFN)-Induced Ubiquitin-like ISG15 Protein. *EMBO J.* **2001**, *20*, 362–371. [CrossRef] [PubMed]

48. Meyer, A.G.; Spielman, S.J.; Bedford, T.; Wilke, C.O. Time dependence of evolutionary metrics during the 2009 pandemic influenza virus outbreak. *Virus Evol.* **2015**, *1*, vev006. [CrossRef]

49. Varga, Z.T.; Grant, A.; Manicassamy, B.; Palese, P. Influenza Virus Protein PB1-F2 Inhibits the Induction of type I Interferon by Binding to MAVS and Decreasing Mitochondrial Membrane Potential. *J. Virol.* **2012**, *86*, 8359–8366. [CrossRef] [PubMed]